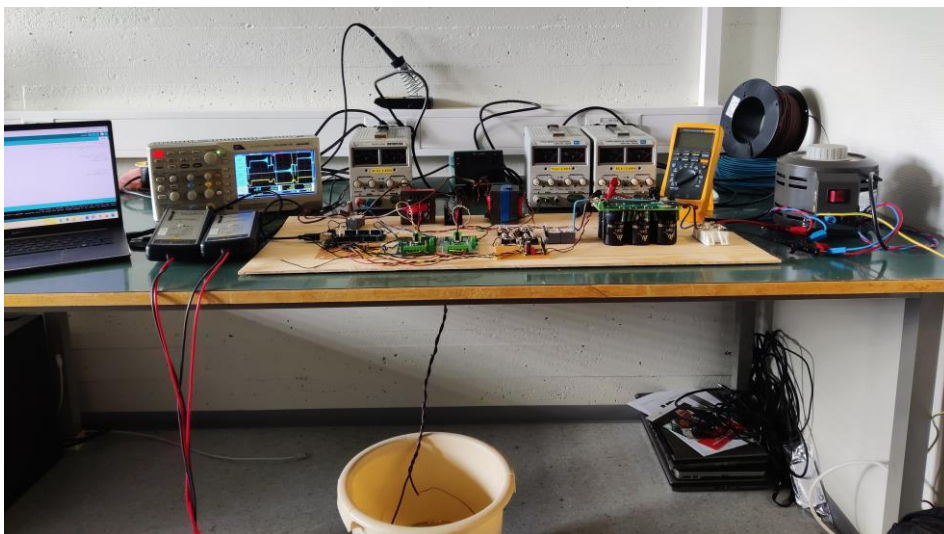# University of South-Eastern Norway

www.usn.no

FMH606 Master's Thesis 2022

Electrical Power Engineering

Design and Control of DC Power Supply for Microbial Electrochemical Synthesis

Elisha Thapa

Faculty of Technology, Natural sciences and Maritime Sciences
Campus Porsgrunn

Course: FMH606 Master's Thesis, 2022

Title: Design and Control of DC Power Supply for Microbial Electrochemical Synthesis.

Number of pages: 78 (69 + Appendices)

Keywords: DC power supply, Bridge rectifier, Switch-mode power supply, Transformer design

Student:	Elisha Thapa
Supervisor:	Kjetil Svendsen
External partner:	Environment Biotechnology Research Group USN-PEM
Availability:	Open

Summary:

Carbon dioxide reduction is one of the major concerns worldwide and the MES is one of the ways for that. It amplifies methane production by reducing the amount of carbon dioxide in the biochemical system.

The thesis centers around the design of an electrically isolated power supply system that can energize a laboratory-scale setup. The electrically isolated system with the half-bridge and full-bridge dc-dc converter is designed and based on the power requirement, the full-bridge dc-dc converter system is investigated closer. Various requisite components are discussed and a centrally tapped transformer suitable for the model is formulated with known parameters. The developed DC power supply model employing a full-bridge dc-dc converter works with 82% efficiency and with the use of proper cables and a cooling system the efficiency can be improved further. It will be connected in a series configuration to provide the necessary power to the MES while at the same time losing less power in the power supply circuit.

Preface

This master's thesis titled "Design and Control of DC Power Supply for Microbial Electrochemical Synthesis" was done under the Electrical Power Engineering department as part of the FMH606 Master's Thesis course at the University of South-Eastern Norway (USN).

The thesis is focused on designing a power supply system that can power up a microbial electrochemical synthesis reactor connected to anaerobic digestion. The microbial electrochemical synthesis increases the production of methane reducing the carbon dioxide production from a biochemical system.

I would like to express my sincere gratitude to my supervisor Kjetil Svendsen for his guidance, encouragement, and support throughout the period of this thesis. He was always available when I needed help and I benefited a lot from his guidance and knowledge to carry out this study. It was a highly valuable experience for me to work under his close supervision. I would like to thank Prof. Carlos Dinamarca and Ph.D. Research Fellow Vasan Sivalingam for their valuable suggestions and support for the thesis work. I would also like to thank my friends Dhanush and Ashim for their support and encouragement. At last, I extend my gratitude to the Electronics and Mechanical laboratories for providing all different equipment such as dc-power supply, multimeter, oscilloscope, workspace, etc. required for designing the supply system.

Porsgrunn, 18.05.2022

Elisha Thapa

Contents

List of Figures

List of Tables

Nomenclature

Abbreviation	Explanation
AC	Alternating Current
AD	Anaerobic Digestion
BES	Bioelectrochemical System
DC	Direct Current
HF	High Frequency
IDE	Integrated Development Environment
IEA	International Energy Agency
IGBT	Insulated Gate Bipolar Transistor
LED	Light-emitting Diode
MEC	Microbial Electrolysis Cell
MES	Microbial Electrochemical Synthesis
MOSFET	Metal-Oxide-Semiconductor Field-Effect Transistor
PWM	Pulse-width Modulation
USB	Universal Serial Bus

1 Introduction

The emission of carbon dioxide (CO_2) is one of the major concerns of environmentalists nowadays as it has a massive contribution to global warming and other environment-related problems. According to the International Energy Agency (IEA) around $33Gt$ (Gigatonne) of CO_2 has been discharged each year from 2017 to 2019 [1]. As a result, direct utilization of CO_2 and conversion of CO_2 into chemicals and energy products methods have emerged. Among two microbial electrosynthesis (MES) is latter type approach which uses bioelectrochemical techniques to convert CO_2 into valuable products using electricity as the energy source [2].

1.1 Background

The MES is a novel technology combining electrical, environmental, and chemical engineering disciplines. It is a power to gas technology that seeks to convert CO_2 into organics that can be used as fuels or building blocks for new products to replace the use of fossil oil and gas. The MES processes are conducted in bioelectrochemical systems (BESs) consisting of an anode and a cathode. An oxidation process occurs at the anode whereas a reduction process happens at the cathode and these electrodes are surrounded by an electrolyte.[2] [3]

The research group at the Department of Process, Energy and Environmental Technology at the University of South-Eastern Norway (USN) has conducted experiments to increase the methane content in biogas produced by biogas upgrading where biogas CO_2 is reduced to methane (CH_4). The experiment uses electricity as an energy source and microorganisms as the catalyst for the chemical reduction reaction ($CO_2 - CH_4$) at the cathode in a methane producing microbial electrolysis cell (MEC). In MEC power is supplied to amplify the kinetics of the reaction and/or to drive thermodynamically unfavorable reactions [4].

For biogas upgradation, it is preferable to have an optimal power supply system that can power up the biochemical system. This thesis work focuses on the design, control, and optimization of the DC power supply system capable to deliver power at the desired level.

1.2 Previous Work

MES seems to have a steady rise in the number of scientific research and publications over the last two decades covering a wide range of domains like chemical synthesis/catalysis, energy production, water treatment, sensors, etcetera. Despite recent improvements, MES remains a long way from being integrated into real-world and commercial applications. [5]

The thesis report of the year 2020 published by USN, centers around the design of various DC power supplies for MES. Several power supply models have been simulated with different configurations such as direct connection and series connection. The report concluded that the switch mode DC power supply is a proper choice, precisely half-bridge DC-DC converter with electrical isolation with series configuration is recommended due to better efficiency and possibility for regulation. [6]

This thesis work is the extension of the previous thesis[6], where an electrically isolated power supply system with a half-/full-bridge DC-DC converter will be designed and regulated using Pulse-width modulated (PWM) signals.

1.3 Objectives

The main goal of the thesis is to design a DC power supply suitable to power up MES connected to an anaerobic digestion (AD) reactor with high efficiency and low power loss within the power supply model. To achieve this goal, the study is divided into flowing tasks:

1. Literature research into half and full-bridge DC converters, transformers, and active rectifiers.
2. Design of half-bridge DC-DC converter with electrical isolation power supply that can be used for a small-scale laboratory setup.
3. Modeling and simulation of the power supply with simulation software.
4. Control and optimization of the power supply output by reducing losses in the system.
5. Build the power supply system operatable at low voltage and perform relevant tests with the reactor if enough time is available.
6. Evaluating the scalability and expansion of the found solution for the full-scale reactor setup.

1.4 Limitation

The power supply system for the MES has several limitations as the process has not been implemented in the real world and this process requires very low DC voltage with the high current flow causing huge energy loss. Some of the limitations are listed below:

i. Power supply to the electrodes is only focused on this work, effects of power supply to the bio and chemical part will not be studied.
ii. The measurement of exact power loss across different components will not be investigated.
iii. The power supply model will not be tested by supplying power to the MES reactor.
iv. The designed power supply system will not be able to handle high current for very long periods.

2 Theory

A half-bridge dc-dc converter with an electrical isolation power supply system has an efficiency of around 92% which is sectioned and connected in series according to the previous thesis work [6]. This thesis focuses on the design and development of a similar power supply with a half-bridge and then with a full-bridge dc-dc converter as the power transmission will be in the range of $2 - 3\ kW$ [7]. Hence, this chapter concentrates on the theory behind the DC power supply system and the different electronics devices utilized in the system.

2.1 DC Power Supply

A power supply is a system that supplies electric power to the electrical load. The MES requires an unregulated AC to be converted to constant DC, in order to operate. However, the supply provided from the mains is fluctuating and has a higher voltage capacity than the limit of the reactor. A regulated dc power supply system converts an unregulated AC to a limited DC to produce constant output. Most of the power supply provides regulated output, isolation, and multiple outputs. There are two designs of DC power supplies: linear DC power supply and switching DC power supply.

2.1.1 Linear DC Power Supply

Linear power supplies are usually heavy as it uses a large transformer, are durable, and have low noise across low and high frequencies. As a result, these supply systems are most suitable for lower power applications where the weight of the system is not an issue. The disadvantages of the systems are size, weight, and low efficiency.[8] [9]

2.1.2 Switching DC Power Supply

Switching power supplies are more efficient, much lighter, smaller in size, and have limited high-frequency noise due to design making them not suitable for high-frequency audio applications. In switching power supplies, the dc voltage is transformed from one level to another via dc-to-dc converter circuits. The power supply system regulates the output voltage via pulse width modulation (PWM). The PWM process enables the switching power supplies to be built with very high-power efficiency and a small form factor. [8] [9]

Figure 2-1 below shows the block diagram of a dc-dc converter system.
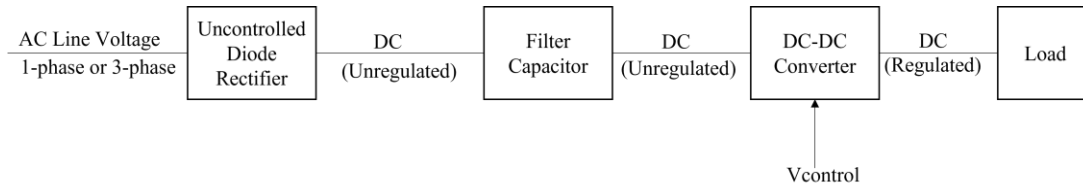
Figure 2-1 DC-DC converter system

2.2 Step-Down Converter

A step-down converter is also known as a buck converter, and it is one of the basic converter topologies. The output voltage level of the step-down converter is lower than the input dc voltage. Figure 2-2 presents a step-down converter for a purely resistive load. The converter takes input dc voltage V_d and generates dc output voltage V_o with desired amplitude by varying the duty ratio of a switch. The duty ratio (D) can be defined as the ratio of the on duration to the switching time period and is given by equation (2.1):

$$D = \frac{t_{on}}{T_s} \tag{2.1}$$

Where, D = Duty ratio

t_{on} = switch on duration

$T_s = (t_{on} + t_{off})$ switching time period

t_{off} = switch off duration

When the switch is on, the diode becomes reverse biased and the input supplies energy to the inductor as well as to the load. During the off-time of the switch, the inductor current flows through the diode transferring some of its stored energy to the load. The low pass filter consisting of an inductor and a capacitor is used to reduce the fluctuations and switching frequency ripple in the output voltage. [9]

The output of the step-down dc-dc converter is derived by averaging the voltage v_{oi} with zero average voltage across the inductor in steady-state as described by equation (2.2)

$$\frac{V_d t_{on} + 0.\, t_{off}}{T_s} = V_o$$

$$V_o = DV_d \tag{2.2}$$

Where, V_0 = DC output voltage

V_d = DC input voltage

D = Duty cycle of the switch
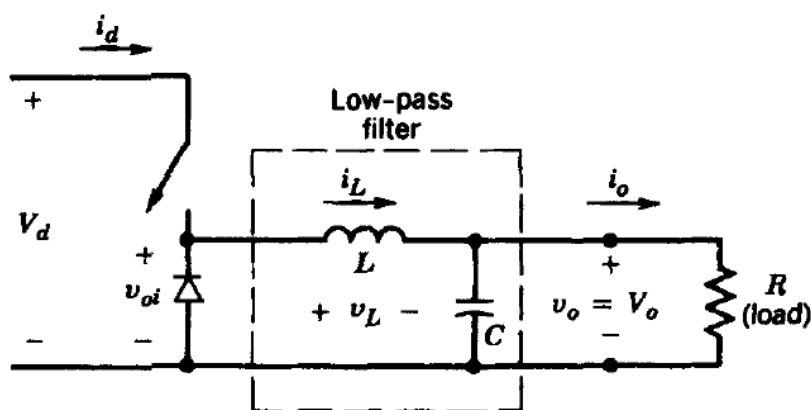
Figure 2-2 Step-down dc-dc converter [9]

2.3 Step-Up Converter

A step-up converter also called a boost converter produces an output voltage greater than the input voltage of the converter. It is also a basic converter topology, which is often derived into other converter topologies depending on the purpose of the converter. It's one of the main applications is in regulated dc power supplies. Figure 2-3 shows the basic circuit diagram of the step-up dc-dc converter. When the switch is on, the diode is reverse biased and the input supplies energy to the inductor, however when the switch is off, both the input and the inductor supply energy to the load. [9]
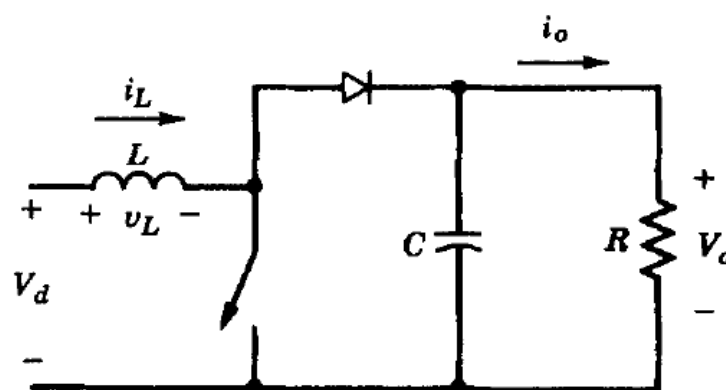
Figure 2-3 Step-up dc-dc converter [9]

2.4 DC-DC Converters with Electrical Isolation

A high frequency (HF) isolation transformer is applied to provide electrical isolation in dc switching power supplies. At first, the ac input voltage is converted to unregulated dc output by utilizing a diode rectifier, then the output is fed to dc-dc converter block with isolation to obtain desired dc output voltage as shown in figure 2-4. In the switch-mode dc-dc converter with isolation, the high magnetizing inductance of the transformer is preferable to reduce the magnetizing current which flows through the switches. Similarly, minimum leakage inductances of the windings are useful for the power supplies. PWM is used to control power transistors or MOSFETs operating as a switch. There is a different type of dc-dc converters with isolation which can be divided into two categories based on the utilization of a transformer core: [9]

    i.   Unidirectional core excitation
   ii.   Bidirectional core excitation
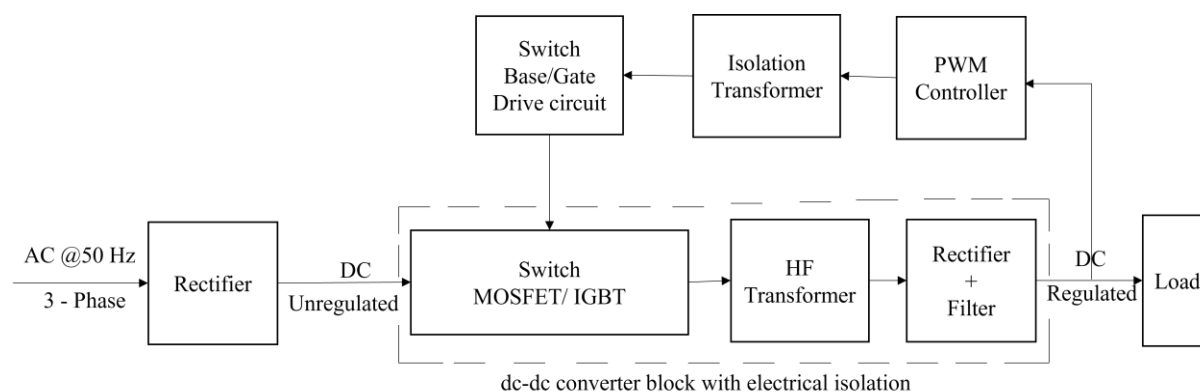
Figure 2-4 Block diagram of a switch-mode dc power supply

i.   Unidirectional Core Excitation

The switching mode dc-dc converters with isolation which utilizes only the positive part i.e., quadrant I of the hysteresis (B-H) loop shown in figure 2-5 are unidirectional core excited converters. It includes flyback and forward dc-dc converters, and the output voltage is regulated by PWM switching scheme. [9]

ii.   Bidirectional Core Excitation

In case of bidirectional core excitation, dc-dc converters with isolation use both positive (quadrant I) and the negative (quadrant III) of the hysteresis (B-H) loop alternatively. Push-pull, half-bridge, and full-bridge dc-dc converters use bidirectional core excitation characteristics of the transformer core. [9]
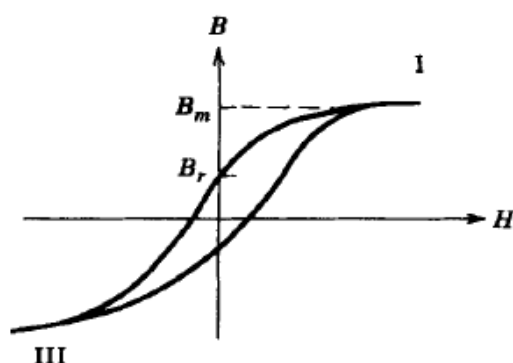
Figure 2-5 Hysteresis (B-H) loop of transformer core [9]

2.5 Half-Bridge DC-DC Converters

A half-bridge dc-dc converter is derived from the step-down converter which has the ability to supply an output voltage either higher or lower than the input voltage. It provides electrical isolation by using a transformer. Figure 2-6 shows a schematic of the converter topology, where capacitors on the primary side produce a mid-point voltage between zero and the input dc voltage across the primary winding. The switches T_1 and T_2 are turned on alternatively for each interval of t_{on} supplying half input voltage to the primary side. The diodes in antiparallel with the switches are for switch protection. The advantage of this topology is the full utilization of the core flux and the secondary winding. Also because of the electrical isolation it separates the input and output circuit, protecting components as well as personnel on the output side. [9] [10]

The average output voltage (V_o) of the half-bridge converter can be calculated as per equation (2.3):

$$V_o = V_d \frac{N_2}{N_1} D \qquad (2.3)$$

Where, V_d = DC input voltage

D = Duty ratio of switches ($D = \frac{t_{on}}{T_s}$ and $0 < D < 0.5$)

$\frac{N_2}{N_1}$ = secondary to primary turns ratio of transformer
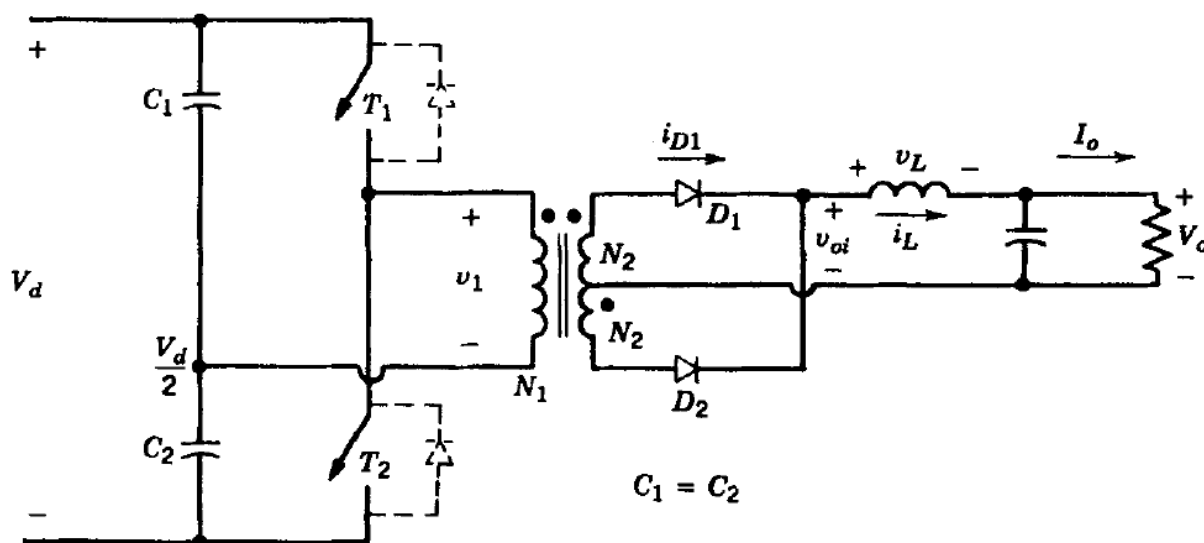
Figure 2-6 Half-bridge dc-dc converter with electrical isolation [9]

2.6 Full-Bridge DC-DC Converter

A full-bridge converter is also derived from the step-down converter, and it can either step up or down the output voltage. The schematic of a full-bridge dc-dc converter consists of four switches (T_1, T_2, T_3, T_4), an isolation transformer, diodes, and output circuit with LC filter and load as seen in figure 2-7. The basic operation involves switching of pair of transistors (T_1, T_2) during a one-half cycle of input and the other pair (T_3, T_4) during the other half of the input voltage. When one pair of switches conducts, the other remains in the off state. The current flows in the opposite directions during alternate half cycles causing the core flux to swing from negative to positive. Hence the full-bridge converter utilizes both positive (quadrant I) and negative (quadrant III) portions of the hysteresis loop, thereby reducing the chances of core saturation.[7] [9] [11]

The RMS currents on the primary and secondary sides can be expressed as equations (2.4) and (2.5):

$$On \; Primary \; side, \qquad I_{1,RMS} = \frac{N_2}{N_1} I_{o,max} \sqrt{D} \qquad\qquad (2.4)$$

$$On \; Secondary \; side, \qquad I_{2,RMS} = I_{3,RMS} = \frac{1}{2} I_{o,max} \sqrt{1 + D} \qquad (2.5)$$

Where, $I_{o,max}$ = maximum output current

18

D = duty cycle

$\frac{N_2}{N_1}$ = secondary to primary turns ratio of transformer
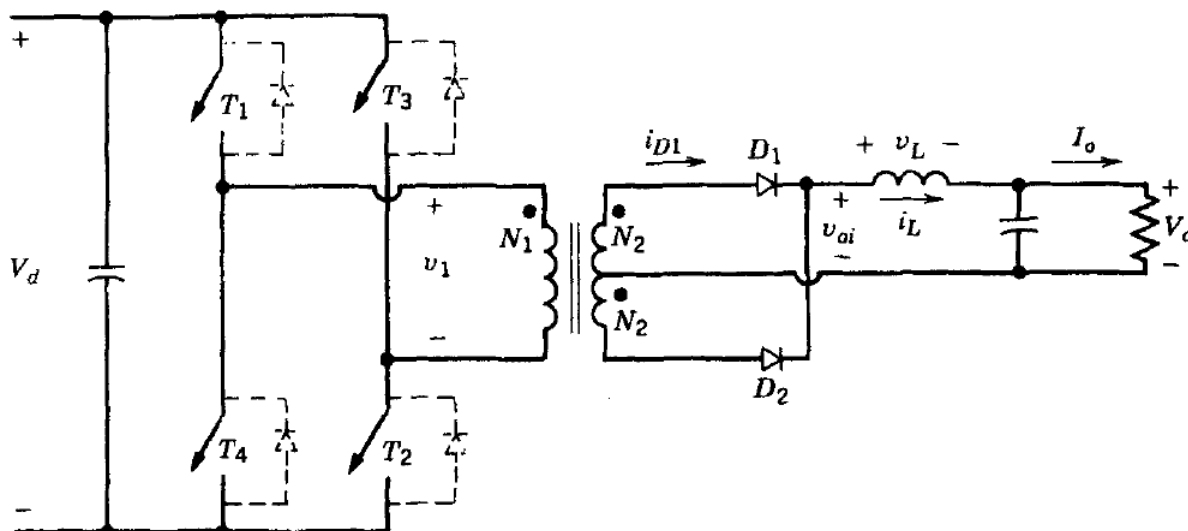
Figure 2-7 Full-bridge dc-dc converter with electrical isolation [9]

The resulting output voltage (V_o) is dependent on the transistor's respective on-state time and it can be derived by integrating the voltage v_1 over time period T_s and then divide it by T_s. The equation (2.6) gives the average output voltage of the full-bridge converter.

$$V_o = 2 \times V_d \frac{N_2}{N_1} D \qquad (2.6)$$

Where V_d = input dc voltage

duty cycle (D): $0 < D > 0.5$

2.7 PWM Switching for Control of DC-DC Converters

PWM switching is a frequently used method for controlling the output voltage of the switching dc power supplies. The average output voltage of the converters depends on the switch on and off duration (t_{on}, t_{off}). In this method, on duration of switch/es is adjusted to control the output at a constant switching frequency keeping a constant switching time period $(T_s = t_{on} + t_{off})$. The duration of the switch is commonly known as variation of switch duty ratio D, which is the ratio of the on duration t_{on} to the switching time period T_s. [9]

The PWM signal is generated by a comparison of a control voltage signal with a repetitive waveform such as a sawtooth waveform as shown in figure 2-8. The switching frequency is obtained from the frequency of the sawtooth waveform, and it is kept constant and chosen in a range of a few kilohertz to a few hundred kilohertz.[9]
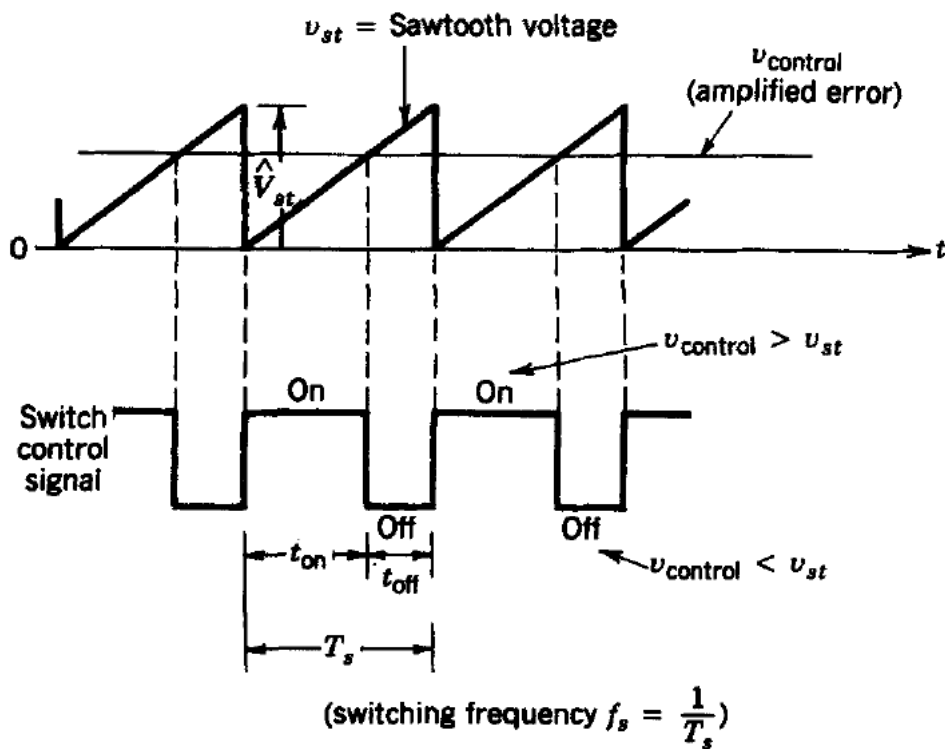
Figure 2-8 PWM signal generation [9]

3 System Overview and Components

The previous thesis [6], analyzed different power supply systems in Simulink and concluded that the half-bridge dc-dc converter with electrical isolation is preferable and has an efficiency of 92% with series configuration. Also, the input configuration for the power supply system is used as previously suggested by a discussion with the research group. There are three different setups of the MES system, and the required inputs are shown in table 3-1 [6] [12]. This thesis focuses on the power supply design for lab-scale setup, hence the power supply system will transfer power around $2 - 3\,kW$. Furthermore, the thesis [6] deduces that the series configuration provides higher efficiency than the direct connection of the power supply to the whole load. Hence the load/MES will be sectioned into 10 parts, the power will be supplied to those loads individually and the whole system will be connected in series. For the lab-scale setup, each power supply will provide voltage of $20\,V$ and current of $100\,A$ with an output power of $2000\,W$. [6]

Table 3-1: Input/Output Configuration for different types of MES [6]

Parameter configuration for different setups of MES					
Setup	**Voltage [V]**	**Current [A]**	**Current density [A/m^2]**	**Anode area [m^2]**	**Power [W]**
Small scale	$1-3$	7.5×10^{-3}	2.5	0.003	$(7.5 - 22.5) \times 10^{-3}$
Lab scale	$1-3$	1000	2.5	400	$1000 - 3000$
Pilot scale	$1-3$	50000	2.5	20000	$50000 - 150000$

3.1 Components of Power Supply System

3.1.1 Rectifiers

Rectifiers convert an alternating current (AC) into a direct current (DC) by using devices such as electron tubes, vibrators, solid-state devices, or mechanical devices [13]. Commonly diodes are used for rectification purposes. When both polarities of an alternating current are used to

produce a direct current then the process is called full-wave rectification whereas the use of only one polarity for direct current is called half-wave rectification. In the case of three-phase ac voltages, three-phase rectifier circuits are suitable as it has a higher power handling capability and lower ripple content in the waveforms. A three-phase rectifier with six diodes and a filter capacitor on the dc side is shown in figure 3-1. The diodes D_1, D_3, D_5 becomes forward biased during positive half ac cycles and the other three diodes D_4, D_6, D_2 conducts in the forward direction during the negative half of ac. The smoothing capacitor C_d is used to make full wave rippled output into more smooth dc output.
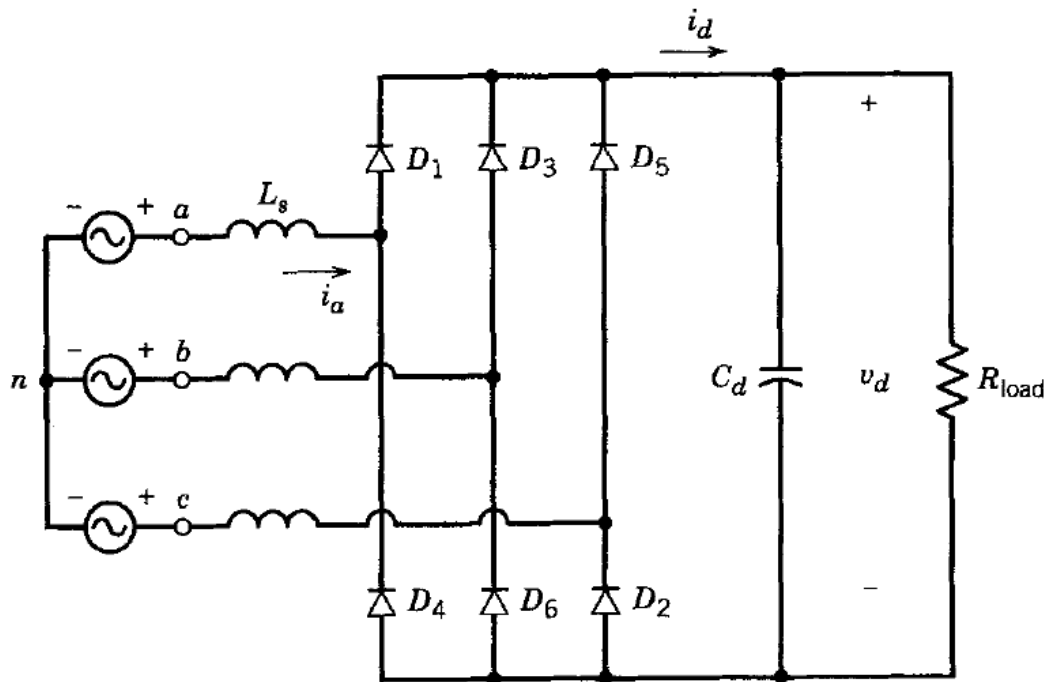
Figure 3-1 Three-phase full bridge rectifier [9]

3.1.2 Diodes

A diode is a semiconductor device with two terminals that conducts current only in one direction. In the case of an ideal diode, it will have zero resistance in one direction while infinite resistance in the other, however, it is not achievable in practice. Instead, the diode has negligible resistance in one direction allowing the flow of current and very high resistance in the reverse direction to prevent current flow. Figure 3-2 shows the diode and its $i - v$ characteristics and ideal characteristics.
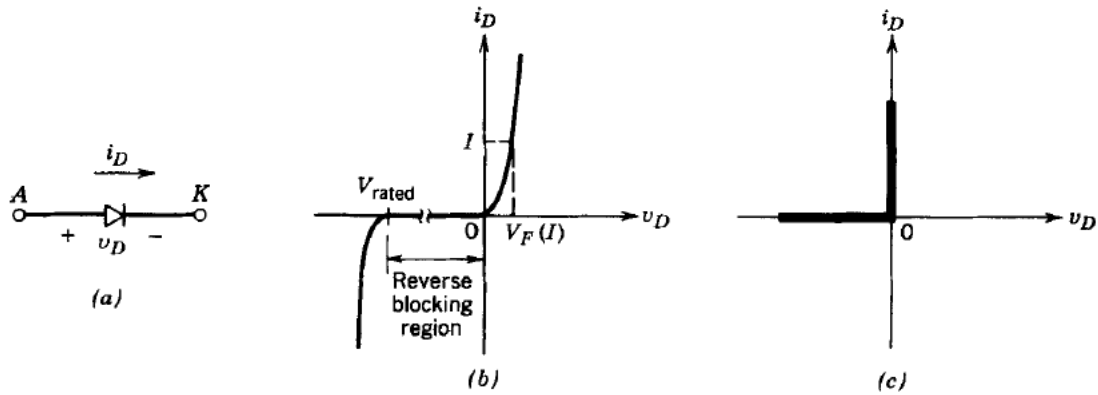
Figure 3-2 Diode (a) symbol, (b) $i - v$ characteristic, (c) idealized characteristic [9]

When the diode is forward biased, it starts to conduct with an only small forward voltage across it, which is in the range of $1\ V$ [9]. The forward voltage (V_F) is almost constant independently of the current level due to the steep characteristics. When the diode is reverse biased, only a small leakage current flows though it until the reverse break-down voltage is reached. All the diode has a maximum reverse voltage (V_{rated}) limit. If the voltage limit is exceeded i.e., the voltage reaches reverse breakdown voltage, then breakdown occurs where the diode conducts a large current in the reverse direction. [9]

The diode can be considered an ideal switch during turn-on as it turns on quickly. This is not the case at turn-off since the current reverses for a reverse-recovery time t_{rr} before falling to zero as shown in figure 3-3. This reverse recovery current is necessary to remove the excessive carriers in the diode and it will introduce the energy loss Q_{rr} at each turn-off. [9]
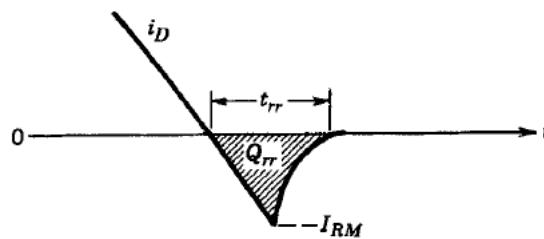
Figure 3-3 Turn-off characteristics of diode [9]

Different diodes depending on the application requirements are described below [9]:

i.   Schottky diodes

Schottky diodes have a very low forward voltage drop of around $0.3\ V$ and are normally used in applications with very low output voltage.

ii.   Fast-recovery diodes

These diodes are designed to have a very small reverse-recovery time and are typically used in high-frequency circuits in combination with controllable switches.

iii.   Line-frequency diodes

These diodes are designed to have on-state voltage as low as possible, resulting in greater reverse-recovery time and it is suitable for line-frequency applications.

3.1.3 Metal Oxide Semiconductor Field Effect Transistors

Metal-oxide-semiconductor field-effect transistors (MOSFETs) are voltage-controlled devices with significant on-state current-carrying capacity and off-state voltage-blocking capacity, thus widely used for switching purposes in power electronic applications. The MOSFET has three terminal sources (S), gate (G), and drain(D) and it can either n-channel or p-channel MOSFETs depending on the doping techniques. The electrical current flowing between the source (S) and drain (D) contacts is efficiently controlled with voltage being applied via the gate (G). Figure 3-4 shows the circuit symbols of N-channel and P-channel MOSFETs, and the arrow heads show the direction of current flow.
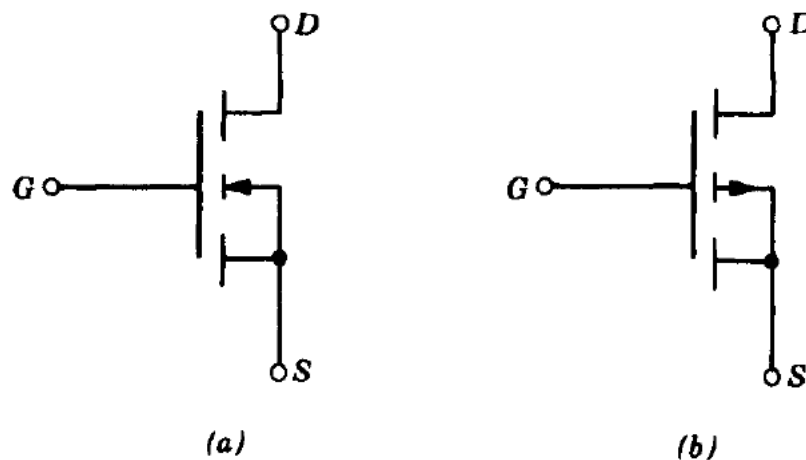
Figure 3-4 Circuit symbols for (a) n-channel and (b) p-channel MOSFETs [9]

Both the n-channel and p-channel MOSFETs have two basic forms: depletion and enhancement modes.

i.   Depletion-mode MOSFET

 The depletion-mode MOSFET is not common as enhancement-mode type MOSFETs. These types of MOSFETs are usually switched 'ON' without the gate bias voltage, i.e., the channel conducts when gate-source voltage (V_{GS}) is zero making them closed devices. [14]

ii.   Enhancement-mode MOSFET

The enhancement-mode MOSFETs are the most common type which is the reverse of the depletion-mode type MOSFETs. These MOSFETs do not conduct i.e., 'OFF' when the gate-source voltage (V_{GS}) is equal to zero. [14]

The current-voltage ($i - v$) characteristics of n-channel enhancement-mode MOSFET is shown in figure 3-5. Enhancement-mode MOSFETs have low 'ON' resistance and very high 'OFF' resistance as well as extremely high input resistance due to their isolated gate, making them suitable for switching operations.
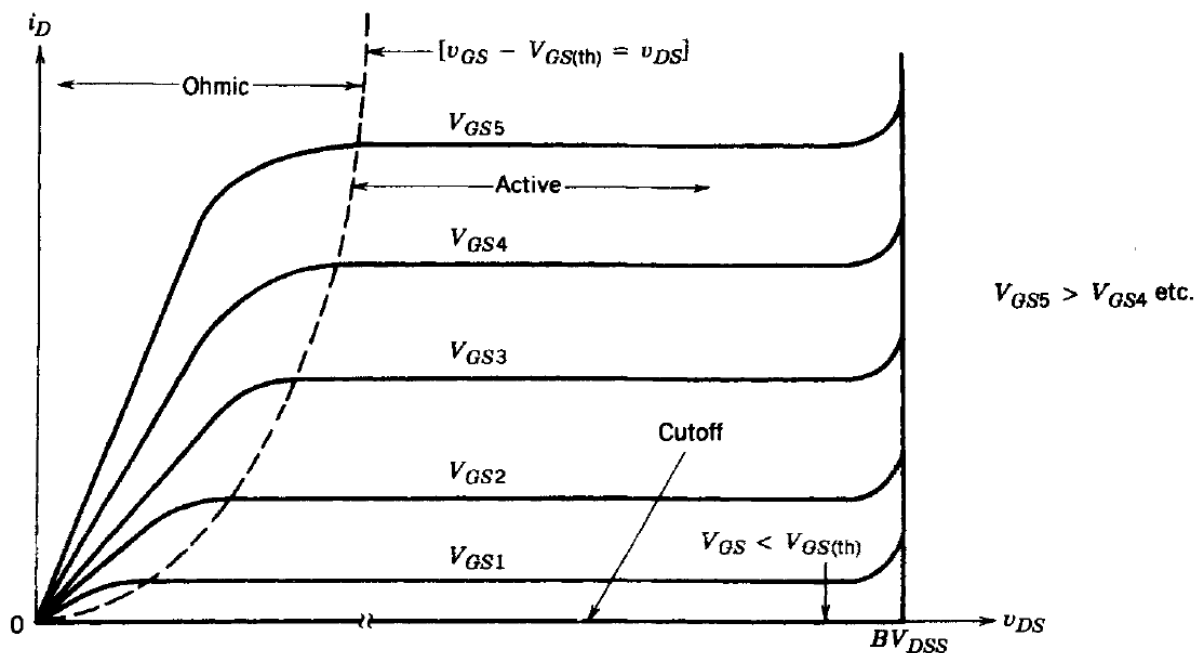
Figure 3-5 $i - v$ characteristics of n-channel enhancement mode MOSFET [9]

The MOSFETs operate within three different regions:

1. Cutoff Region: The MOSFET is in the cutoff region when the gate-source voltage (V_{GS}) is less than the threshold voltage ($V_{GS(th)}$) i.e., $V_{GS} < V_{GS(th)}$. The device act as an open switch regardless of the value of v_{DS} with drain current (i_D) = 0.
2. Ohmic (Linear) Region: The MOSFET is in the ohmic region when it is driven by a large gate-source voltage (V_{GS}) where the drain-source voltage (v_{DS}) is small i.e., $V_{GS} - V_{GS(th)} > v_{DS} > 0$. The transistor behaves as a voltage-controlled resistance whose resistive value is determined by the gate voltage (V_{GS}) level.
3. Active (Saturation) Region: The MOSFET is in the active region or constant current region when $V_{GS} > V_{GS(th)}$ and $v_{DS} < V_{GS}$. The drain current (i_D) is independent of the drain-source voltage (v_{DS}) and only depends on the gate-source voltage (V_{GS}).

3.1.4 Insulated Gate Bipolar Transistors

Insulated gate bipolar transistors (IGBTs) are voltage-controlled devices which is cross between conventional bipolar junction transistors and field-effect transistors making them suitable for switching. The IGBT combines the best features of these two types of transistors, the high input impedance and high switching speeds of a MOSFET with a low saturation voltage of a bipolar transistor to create a transistor capable of handling large collector-emitter currents with virtually zero gate current drive [15]. The IGBT has three terminals gate (G), collector (C), and emitter (E) as seen in figure 3-6. It can be turned 'ON or 'OFF' by activating and deactivating the gate (G) terminal. The IGBT will be 'ON' if a positive input voltage signal is applied across the gate and emitter but when the input gate signal is zero or negative then it will be turned 'OFF'.
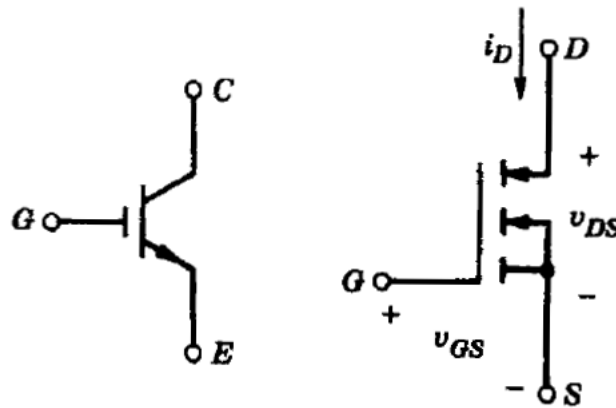
Figure 3-6 Circuit symbol of n-channel IGBT [9]

The IGBT is unidirectional which switches current only in the forward direction from the collector (C) to the emitter (E) unlike MOSFETs which are bidirectional transistors. The operation of IGBT is immensely close to that of n-channel power MOSFET and $i - v$ characteristics are also very similar which is illustrated in figure 3-6 [15]. The IGBT is in the off state when v_{GS} is less than the threshold voltage $V_{GS(th)}$. As in the figure 3-7, the curve is nearly linear for most of the drain current (i_D) range and it becomes nonlinear only when v_{GS} approaches the threshold voltage at low drain currents.
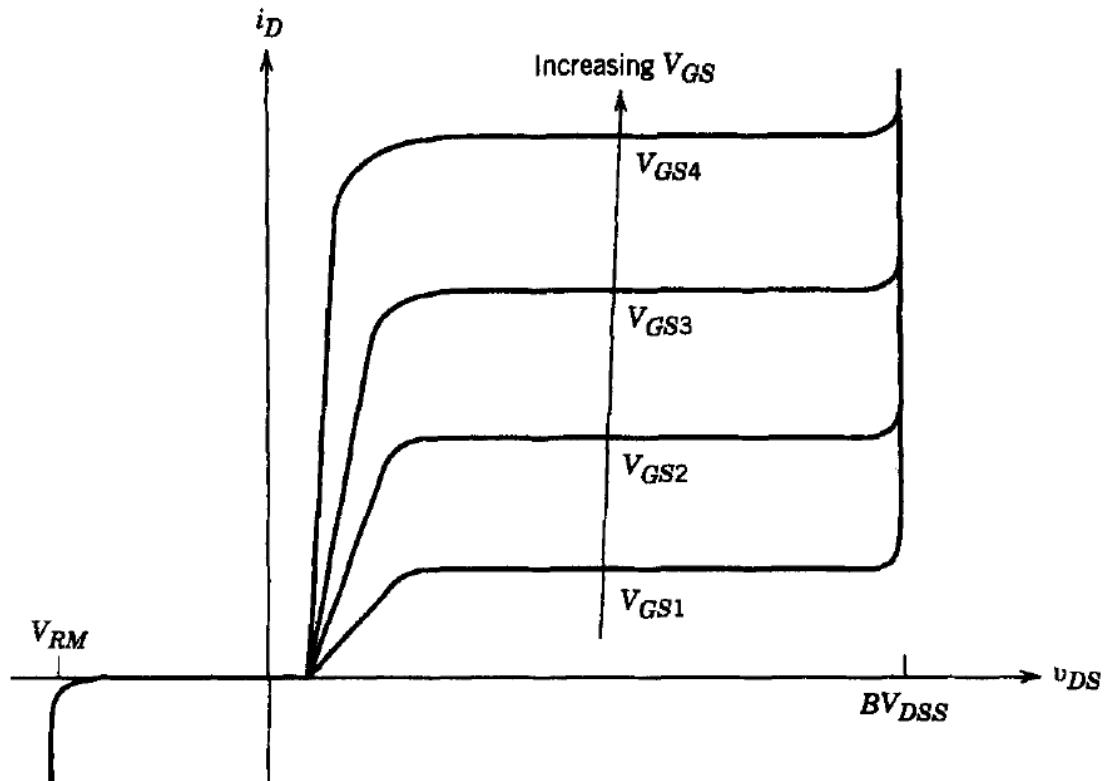
Figure 3-7 $i - v$ characteristic of n-channel IGBT [9]

3.1.5 Gate Drive Circuits

The main function of a drive circuit is to switch a power semiconductor device from the off-state to the on-state and vice versa. It is an interface between the power switches and the control circuit. The MOSFETs and IGBTs are voltage-driven devices with insulated gates, which require gate drive circuits for switching. The drive signals can be directly coupled to the power switch or electrically isolated drive circuits can be used between the logic/control circuit and power switch. The isolation can be obtained via using optocouplers, optic fiber cables, or a transformer. Figure 3-8 below shows the electrically isolated drive circuits by using a transformer. The drive circuits are connected in parallel with the power switch terminals.[9]
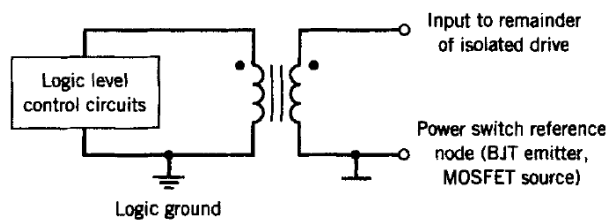
Figure 3-8 Electrically isolated gate drive utilizing a transformer [9]

3.1.6 Arduino

Arduino is an open-source platform consisting of both a microcontroller and software or Integrated Development Environment (IDE) to send instructions to the microcontroller. The Arduino IDE uses a simplified version of C++, and it runs on Windows, Mac, and Linux operating systems. Most of the Arduino boards have Atmel 8-bit AVR microcontrollers such as ATmega1280, ATmega2560, etc. with different features, flash memory, and pins [16].

Arduino Mega ADK consists of an ATmega2560 microcontroller chip and has a USB (Universal Serial Bus) to host interface as shown in figure 3-9. It can be powered up using a USB connection or with an external power supply. An ac-to-dc adapter should be used while supplying power from an external ac source and the best input voltage range is $7 - 12\ Volts$. The Arduino board has 16 analog inputs, 4 hardware serial ports, a $16\ MHz$ crystal oscillator, a power jack, a USB connection, a reset button, and 54 digital input/output pins of which 15 can be used as PWM outputs. [17]
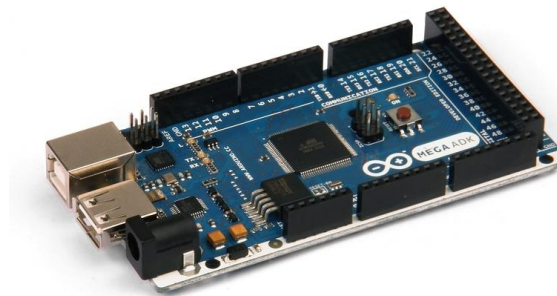
Figure 3-9 Arduino Mega ADK [16]

3.1.7 Transformer

Transformer transfers energy from one circuit to another either increasing (stepping up) or reducing (stepping down) the voltage and it consists of two or more coils that are magnetically coupled. It uses the principle of electromagnetic induction i.e., as the magnetic lines of force (flux lines) build up and collapse with the change in current passing through the primary coil, current and voltage are induced in another coil called the secondary coil. The primary and secondary coil/windings are electrically isolated from each other and are linked magnetically via the common core.

Transformers are used in various applications and they are not commercially available in a wide range of properties but can be designed and constructed for a particular application [9].

For the power supply being studied in this thesis, a high-frequency transformer is required as the switching frequency will be high.

3.1.7.1 Core Materials

One type of core material consists of alloys of iron a small amounts of other elements including chrome and silicon are called soft iron cores. They can withstand a high level of a magnetic field as it has a large value of saturation flux density of around $1.8\,T$. These cores are only suitable for use in low-frequency applications as it has high eddy current losses leading to undesirable heating of the core. The cores must be laminated to reduce the eddy current loss even at modest frequencies. [9]

Powdered iron cores consist of small iron particles that are electrically isolated from each other to increase the resistivity higher than in laminated cores and also thereby reducing eddy currents. It can be used for higher frequencies. [9]

METGALs is an amorphous metal with roughly 70-80 atomic percent iron and other transition metal elements and around 20 atomic percent boron and other forming elements. The electrical resistivity of these cores is somewhat larger than most magnetic steels and has a saturation flux density of $0.75\,T$ at room temperature and $0.65\,T$ at $150\,°C$. [9]

Ferrite core is basically a mixture of iron oxide and different kinds of metal oxides. It has high electrical resistivity but low saturation flux densities around $0.3\,T$. The cores have significantly high permeability, allowing low loss operation with really high frequencies. The electrical resistivity is also high so there are no significant eddy current losses. Due to this, it is the best core choice for an application operating at frequencies higher than $10\,kHz$. [9]

3.1.7.2 Transformer Design Procedure

A suitable transformer design is a vital part of the power supply circuit as it is not available off the shelf in the exact same parameter that suits the power supply system being designed in the thesis. As the switching frequency will be higher in the circuit, ferrite cores are the best choice. The cores have different shapes and sizes such as toroids, pot cores with an airgap, and U, E, and I shape. A bobbin or a coil former comes with most cores and has an effective width which is essential to calculate the wire diameters and the construction of the transformer. They are also available in various shapes and sizes. [9] [18]

Litz wire is suitable for high-frequency applications as it reduces skin effect and proximity effect losses. It also increases the efficiency of high-frequency transformers, inductors, and coils. The Litz wire is composed of several thin individually insulated copper wires that are twisted or woven together in specified patterns which is completely different from simply twisting the copper strands together. [19]

Step 1 Assemble design inputs

The design inputs consist of the input voltage range on the primary side, the output voltage on the secondary side, output current, switching frequency, operating mode, transformer turn ratio, and maximum duty cycle.

Step 2 Choose core material, shape, and size

The operating frequency, power requirements, and switching topology influence the core choice. Iron powder cores, magnetic steels, and METGALs are suitable for low frequencies whereas ferrite cores are the best choice for high-frequency circuits.

The core shapes play a vital role in the construction of high-frequency transformer designs to minimize losses. The winding area should be wide enough to increase the winding breadth and limit the number of layers [20]. For selecting an appropriate core size, many variables should be considered such as effective core area, available window area for winding, etc.

Step 3 Find the primary and secondary turns

Primary and secondary turns are dependent on each other and are influenced by various parameters. The number of primary turns of the transformer has an effect on the flux density of the core material, it is important to see that the core would not saturate. The number of primary turns (N_{pri}) and the peak flux density of the core ($\hat{B}_{core}$) related as per equation (3.1). [21]

$$V_{pri} = N_{pri}A_c\omega\hat{B}_{core}$$
(3.1)

Where, V_{pri} = Voltage on the primary side

A_c = effective area of the core

The equation (3.1) has been derived from Faraday's law of induction,

$$V_{pri}(t) = N_{pri}\frac{d\emptyset}{dt}$$
(3.2)

Where, $V_{pri}(t)$ = time-varying voltage on the primary side

$\frac{d\emptyset}{dt}$ = time derivative of the magnetic flux in the core

The magnetic flux is given by equation (3.3).

$$\emptyset = A_c \hat{B}_{core} \tag{3.3}$$

From equations (3.2) and (3.3),

$$\int_0^{DT_s} V_{pri}\, dt = N_{pri} A_c \int_0^{B_{core}} dB \tag{3.4}$$

The voltage on the primary side over time from 0 to DT_s is equal to the input voltage of the converter V_d. The maximum voltage applied on the primary side of the transformer will produce the peak flux density of the core ($\hat{B}_{core}$), which can be found in the datasheet of the selected core. Then the equations become:

$$N_{pri} = \frac{V_d DT_s}{A_c \hat{B}_{core}} \tag{3.4}$$

Which can be further simplified to calculate as equation (3.5):

$$N_{pri} = \frac{V_{d,max} D_{max} T_s}{A_c \hat{B}_{core}} \tag{3.5}$$

The equation (3.5) clarifies as the number of primary turns increases then the peak flux density of the core will decrease. The number of secondary turns is calculated from the turn ratio of the transformer as shown in equation (3.6).

$$n = \frac{V_{pri}}{V_{sec}} = \frac{N_{pri}}{N_{sec}} \tag{3.6}$$

Step 4 Choose wire

The selection of conductor wire depends on the operating frequency of the transformer and the importance of eddy current loss in the windings. The RMS currents on primary and secondary windings have a significant role in finding appropriate wiring. The RMS currents on the windings can be calculated using equations (2.4) and (2.5). There are different types of winding conductors such as round wire, Litz wire, and so forth and Litz wire is suitable for high frequency and large primary and secondary currents [9]. To cope with high currents, the bundle of Litz wires has to be used on both the primary and secondary sides. The conducting wire with sufficient current density (J) and cross-sectional area ($A_{c,wire}$) will be chosen for windings, then numbers of wire in a bundle can be calculated as following: [21]

For the primary side, the number of bundled wires (X_{pri}) can be calculated as equation (3.7).

$$X_{pri} = \frac{I_{1,RMS}}{JA_{c,wire}} \ [Int] \tag{3.7}$$

Then, the new cross-sectional area of the bundled wire ($A_{c1,bundle}$) of the primary side is given by equation (3.8).

$$A_{c1,bundle} = X_{pri}A_{c,wire} \tag{3.8}$$

Similarly, the total number of bundled wires (X_{sec}) on the secondary side is determined by equation (3.9).

$$X_{sec} = \frac{I_{2,RMS}}{JA_{c,wire}} \ [Int] \tag{3.9}$$

Then, the new cross-sectional area ($A_{c2,bundle}$) is given by equation (3.10).

$$A_{c2,bundle} = X_{sec}A_{c,wire} \tag{3.10}$$

Step 5 Find the required winding window

The total copper area is a product of the total number of turns in the winding window of the core and the cross-sectional area of the conducting wire. The area of the winding window will be larger than the copper area due to several factors. To calculate the required winding window, the number of turns on both sides and copper fill factor (K_{Cu}) must be known. The copper fill factor ranges from 0.3 for Litz wire to $0.5 - 0.6$ for round wire conductors. [9]

The winding area on the primary side ($A_{w,pri}$) is calculated as equation (3.11).

$$A_{w,pri} = \frac{N_{pri}A_{c1,bundle}}{K_{Cu}} \tag{3.11}$$

Likewise, the winding area on the secondary side ($A_{w,sec}$) can be determined as equation (3.12).

$$A_{w,sec} = \frac{N_{sec} A_{c2,bundle}}{K_{Cu}} \tag{3.12}$$

Hence, the total winding area is a sum of the equations (3.11) and (3.12).

$$A_w = A_{w,pri} + A_{w,sec} \tag{3.13}$$

Step 6 Calculate the winding window of the selected core

The datasheet of the chosen core contains all the necessary measurements to calculate the winding window area.

Step 7 Compare required and calculated winding window

Compare the total winding area required for the design of the power supply system and compare it with the winding area of the transformer core. If the winding window of the selected core is slightly more than the required area, that core can be used otherwise step 2 should be repeated to choose a core with a sufficient winding window.

3.1.8 LC Filter

LC filter is a combination of inductor (L) and capacitor (C) to cut or pass specific frequency bands of an electric signal. In the power supply system, both the voltage and the current need to be filtered which is done by a low pass filter seen in figure 3-10.
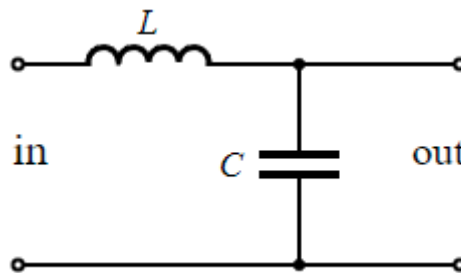
Figure 3-10 Output lowpass filter [22]

The inductor blocks AC components at higher frequencies while the capacitor's impedance decreases and passes high-frequency components. By combining the inductor and capacitor with opposite properties, high-frequency AC components can be prevented, and noise can be cut. The DC power supply system is susceptible to AC ripple and noise, hence lowpass filter between the output of the transformer and load should be placed. The value of the inductor

should be high enough in order to keep the output current ripple within the limit. The current ripple between 5-10% of the average load currents is often accepted. [21] [22]

For the calculation of inductance, inductor current from $0 - DT_s$ is considered. The voltage across the inductor is given by equation (3.14)

$$V_L = L \frac{di_L}{dt} \tag{3.14}$$

Then, the inductance is given by equation (3.15)

$$L = \frac{V_L}{\frac{di_L}{dt}} \tag{3.15}$$

The inductance will be minimum when the voltage across the inductor reaches its maximum value $(V_{L,max})$ as shown in equation (3.16)

$$L_{min} = \frac{V_{L,max}}{\frac{ripple * I_{L,max}}{t_{on}}} \tag{3.16}$$

Then, the voltage over the inductor can be expressed as equation (3.17)

$$V_L = V_{oi} - V_o \tag{3.17}$$

Where, $V_{oi} = \frac{N_2}{N_1} V_d$

The maximum voltage over the inductor is given by equation (3.18)

$$V_{L,max} = \frac{N_2}{N_1} V_{d,max} - V_{o,min} \tag{3.18}$$

The on-state can be determined as equation (3.19)

$$t_{on} = DT_s = \frac{V_{o,min}}{V_{d,max}} \frac{N_2}{N_1} T_s \tag{3.19}$$

The maximum average inductor current is given by equation (3.20)

$$I_{l,max} = \frac{P_{o,max}}{V_{o,max}} \tag{3.20}$$

Hence, the equation (3.16) can be written as equation (3.21) by replacing the value of $V_{L,max}$ by equation (3.18)

$$L_{min} = \frac{\frac{N_2}{N_1}V_{d,max} - V_{o,min}}{\frac{ripple * I_{L,max}}{t_{on}}} \tag{3.21}$$

To calculate the capacitance, the following relation is used

$$i_c(t) = C\frac{dV_c}{dt} \tag{3.22}$$

With the assumption that all the ripple current ($ripple_I$) goes through the capacitor, and the voltage ripple ($ripple_V$) has a constant value, the maximum capacitance value can be calculated as equation (3.23)

$$C_{max} = \frac{i_c(t)}{\frac{dV_C}{dt}} = \frac{ripple_I * I_{L,max}}{\frac{ripple_V * V_{o,min}}{t_{on}}} \tag{3.23}$$

3.2 Power Losses in Switches

Power loss in a switch is the product of the current through the switch and the voltage across it. When the switch is off, there is no current through it although there will be a voltage across it leading to no power dissipation. Similarly, when the switch is on, there is current across it, but no voltage drops across it so no power loss. In the case of actual switches such as IGBT, and MOSFET, it has mainly two types of power loss: conduction loss and switching loss.

Conduction loss (P_C) arises due to the small internal resistance in the transistor causing a small voltage drop across when the switch/transistor is fully on. The loss associated with leakage current is negligible since the leakage current is quite small and does not vary significantly with voltage.

The switch/transistor takes a finite time to turn on and turn off the switch which creates power dissipation known as switching loss (P_{SW}). During the switching time, the switch has a current through it at the same time as the voltage across it resulting in the switching loss.

The switching loss is given by equation (3.24)

$$P_{SW} = P_{on} + P_{off} \tag{3.24}$$

Where, P_{on} = Transistor turn-on losses

P_{off} = Transistor turn-off losses

Hence the total power transistor/switch loss P_t, can be written as equation (3.25)

$$P_t = P_C + P_{SW} \tag{3.25}$$

3.3 Power Losses in Transformer

An ideal transformer does not have energy losses with equal input and output power, however, in practice both the input and output powers will not be the same because of losses within the transformer. There are different types of losses in the transformer such as hysteresis, copper, eddy, and dielectric, described below.

i.   Resistive Loss

The power loss caused by the resistance of the wire used for winding in the transformer is known as a resistive loss, or I^2R loss, or copper loss. The power loss (P) is directly proportional to the resistance of the wire (R), and the square of the current (I^2) though it as shown in equation (3.26). The greater value of either resistance or current, the higher the power loss, so the proper diameter of wire should be used to minimize the loss. Also, the length of primary and secondary windings affects the resistance of the wire.

$$P = I^2R \tag{3.26}$$

Where, $R = \frac{\rho L}{A}$ = resistance of wire with length (L), area (A), and resistivity (ρ).

ii.   Hysteresis Loss

Hysteresis loss is caused by the remaining magnetism in a core material after the magnetizing force has been removed. This kind of loss occurs in the core when the alternating current is

applied then the magnetic field will be reversed. When a magnetic field is passed through the core, it gets magnetized by aligning the magnetic domain in the direction of the field. When the magnetic field reverses, the magnetic domain also reverses its alignment causing power dissipation in the form of heat. The loss can be kept at a minimum value by the use of proper core materials.

If the transformer is loaded beyond its rated capacity, then saturation loss occurs. This happens when the core reaches its saturation point and no additional flux liens are produced while increasing the current through the core. [23]

iii.   Eddy Current Loss

Eddy current loss is power loss due to induced current in the metal parts of the transformer from the alternating current. When the primary side of the transformer is energized by an alternating current, a fluctuating magnetic field is produced. The conducting core material in the moving magnetic field has a voltage and current induced in it. The induced current flows through the core dissipating power in the form of heat. The eddy current loss increases with frequency and is directly proportional to the square of the current in the winding. The loss can be reduced by using laminated iron cores and ferrite cores which have no significant eddy current loss due to high electrical resistivity.

4 Modeling and Simulation

This chapter discusses the power supply system design and simulations.

4.1 Model Formulation in Simulink

Based on previous thesis work [6], the half-bridge dc-dc converter with electrical isolation with series configuration is recommended to supply power to the biochemical system. The power required for the lab-scale setup is around $2 - 3\,kW$ which leads to the use of a full-bridge converter, hence both half-bridge dc-dc converter and full-bridge dc-dc converter in the power supply system are simulated in the MATLAB-based graphical program Simulink.

4.1.1 MATLAB

Matrix Laboratory (MATLAB) is a tool for programming, computation, and visualization integrated with a single environment where problems and solutions are expressed in mathematical notation. It is well suited for matrix and vector formulations, implementation of algorithms, and solving problems related to linear algebra, modeling, simulation, etc. MATLAB has large application-specific toolboxes. [24]

4.1.2 Simulink

Simulink is a MATLAB-based graphical programming environment for modeling, simulating, and analyzing dynamic systems. Simulink provides a graphical user interface (GUI) for creating a system with different system components. It has a comprehensive library of pre-defined components/blocks that can be used to build graphical models of a system by drag-and-drop mouse operations. Simscape and Simscape Electrical libraries are used in this thesis for developing the model of the power supply system. Simscape Electrical library provides components for modeling and simulating electronic and electrical power systems including models of semiconductors, motors, etc. [25]. Simscape library helps to develop a model by assembling fundamental components into a schematic [26].

4.1.3 Models in Simulink

All the components used in the circuit are available in the Simscape Electrical library. The MATLAB and Simulink version used for design and simulation is R2021b. The ode23tb solver has been used to simulate the system in Simulink with default parameters setup and a stop time of 0.05 seconds. A powergui block is essential to simulate any model using components from the Simscape Electrical library [27]. The power supply system with both half-bridge and full-bridge dc-dc converter utilizes the Continuous solver method in the powergui which uses a

variable-step solver from Simulink. The tools and preferences tabs of the powergui block remain as it is.

A three-phase AC source represents the main source with a phase shift of 120 degrees, phase voltage $230\ V$, and frequency $50\ Hz$. The AC supplied voltage is converted to DC through the use of six diodes which work as a rectifier. The default value of the diode is used, which corresponds to internal resistance, Ron of $0.001\ \Omega$, and a forward voltage, Vf of $0.8V$ [28]. The converted DC then goes to two capacitors having a capacitance of $20000\ \mu F$, which is further connected to switches. The MOSFETs/IGBTs are applied as switch for dc-dc converters with default values- The MOSFETs have internal resistance, Ron of $0.1\ \Omega$, internal diode resistance, Rd of $0.01\ \Omega$ and internal diode forward voltage, Vf of $0\ V$ [29] and the IGBTs have resistance Ron of $0.001\ \Omega$ and forward voltage Vf of $1\ V$ [30]. The applied switches are controlled by PWM, which is generated by comparing a sawtooth waveform with a control voltage signal. The sawtooth generator generates the sawtooth with intervals -1 to 1, which is modified in the circuit so that the interval becomes $0 - 1$. The D flip-flop bock is used to send PWM to the switches with help of AND gates. Every time period when the PWM signal is at 0 or OFF then the signal goes to the clock (CLK) port of the flip-flop via NOT block and flips between Q and !Q. All the switches are off under this period of flipping. When the PWM is ON, the flip-flop will send a signal either through Q or !Q then to one of the respective AND gates. The switches will have their respective on-period when the PWM is on, but they will take turns to conduct every on-time period.

The three winding linear transformers with three windings coupled and wounded on the same core have been used for stepping down the voltage and also for electrical isolation between the input and output side [31]. In the case of the transformer, the values are changed from the default values for both half-bridge and full-bridge circuits. The units used in the transformer is SI and a nominal power Pn is $250\ MVA$ and a nominal frequency fn is $50\ Hz$ for both type of dc-dc converter. The magnetization resistance Rm and inductance Lm are also the same for both which have values of $320.01\ \Omega$ and $1.0186\ H$ respectively. The full-bridge dc-dc converter circuit has a winding 1 to winding 2/winding 3 ratios of 10 whereas the half-bridge supply system has half the transformer ratio. A higher number of primary windings or a higher transformer ratio is required in the full-bridge network compared to the half-bridge as the full-bridges see double the voltage than the half-bridge.

The transformer converts the supplied dc voltage to the desired voltage level. The secondary side of the transformer is connected to the rectifier diodes which conduct when forward biased. The output rectifier diodes also have the default parameter values as input rectifier diodes. Then the rectified dc-voltage will be filtered via an LC filter before it reaches the load. The inductor L will filter the remaining ripple in voltage left from the rectification and the capacitor C will smoothen the voltage signal. The inductor and capacitor have default values and the resistor which acts as the load has a resistance of $0.2\ \Omega$.

I. Power supply system with half-bridge dc-dc converter with electrical isolation

The half-bridge dc-dc converter with the MOSFET switch model is shown in figure 4-1. The output values of the system will have a current of around $100\ A$ and voltage of roughly $20\ V$ resulting in the output power of around $2000\ W$. The power supply system will be sectioned with 10 in series to supply the required power to the reactor. The power is measured in different components such as input diodes rectifier, switches, transformer, output diodes rectifier, LC filter, and load in the circuit to calculate the power loss. The total power loss P_{loss} of the system is given by equation (4.1). The power losses are calculated on the input rectifier diode $P_{input\_rectifier}$, switches $P_{switches}$, transformer $P_{transformer}$, output rectifier diodes $P_{output\_rectifier}$ and LC filter P_{LC_filter} as per the method applied in the previous thesis [6].

$$P_{loss} = P_{input\_rectifier} + P_{switches} + P_{transformer} + P_{output\_rectifier} + P_{LC\_filter} \quad (4.1)$$

The power efficiency of the model is given by equation (4.2)

$$Efficiency, \eta = \frac{P_{input}}{P_{output}} \quad (4.2)$$

Where input power is denoted by P_{input} and output power is denoted by P_{output}.

Table 4-1: Power and efficiency of half-bridge power system model

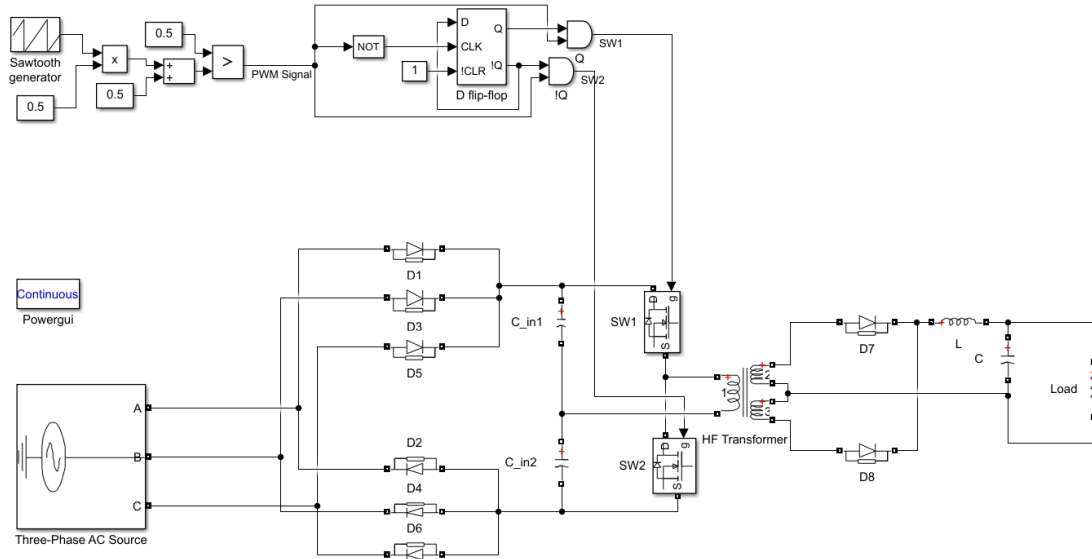| Power Measurement in Half-bridge Model				
Switch	Input Power [W]	Power Loss [W]	Output Power [W]	Efficiency [%]
MOSFET	2310	182	2139	92.6
IGBT	2313	197	2130	92.1

Figure 4-1 Half-bridge dc-dc converter with electrical isolation

II.   Power supply system with full-bridge dc-dc converter with electrical isolation

The power supply system with a full-bridge dc-dc converter has most of the components same as the half-bridge model, however, there are four switches that work on pair as per PWM signal. Figure 4-2 shows the schematic diagram of the power supply system utilizing the full-bridge dc-dc converter. This model will also be connected in a series configuration to provide the power of around $2000\ W$ to the reactor. The total power loss and the efficiency of the system will be calculated as per the equations (4.1) and (4.2) respectively.

Table 4-2: Power and efficiency of full-bridge power system model

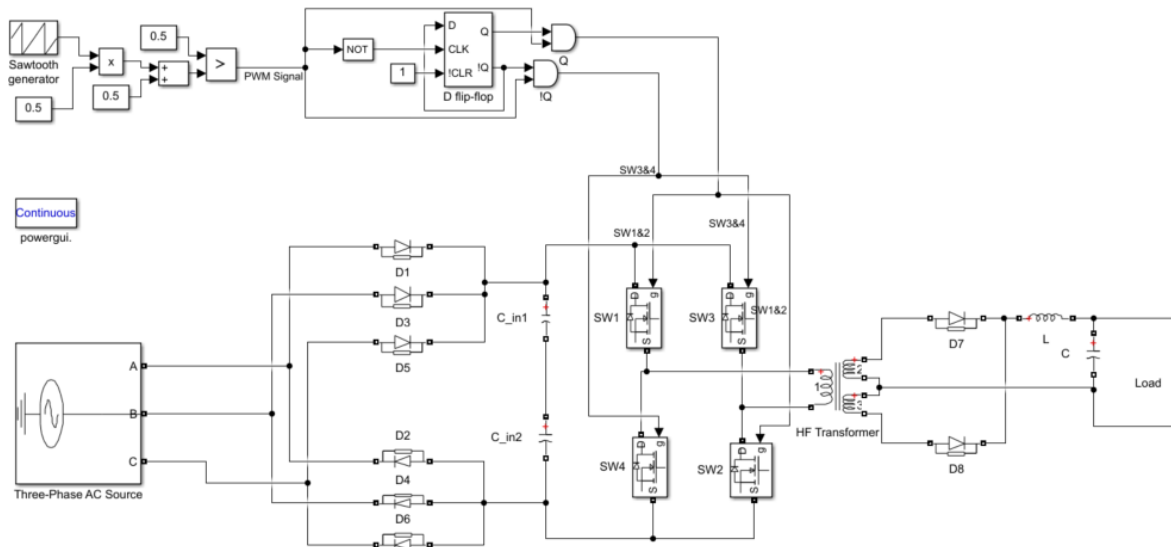| Power Measurement in Full-bridge Model				
Switch	Input Power [W]	Power Loss [W]	Output Power [W]	Efficiency [%]
MOSFET	2388	370.3	2015	84.4
IGBT	2415	370	2043	84.6

Figure 4-2 Full-bridge dc-dc converter with electrical isolation

The power loss and efficiency are calculated using both half-bridge and full-bridge dc-dc reactors with the transformer. As per simulation in the Simulink, the system with a half-bridge converter has an efficiency of around 92%, and that for the full-bridge system is around 84% both for MOSFETs and IBGTs switches. However, the efficiencies and power loss will not be the same in the circuit with actual components as the losses calculated in switches, transformers do not cater for conduction losses, switching losses, magnetization loess, core losses, etc.

4.2 Power Supply System Design

This sub-chapter describes the components used in the power supply circuit and their setups. Figure 4-3 shows the block diagram with different components of the power supply system for MES.

The design started with testing the PWM signals generated from the Arduino by changing the brightness of a LED (Light-emitting diode), then the frequency changing of PWM is done. Figure 4-4 shows the brightness changing test in LED by varying the value of the duty cycle of the pin where the LED is connected. The next step in the design is to select suitable core material for the transformer, proper core shape, and to calculate the numbers of turns on the primary and secondary side, winding window area. After completing the proper transformer setup, all the required components are gathered for creating the power supply system.
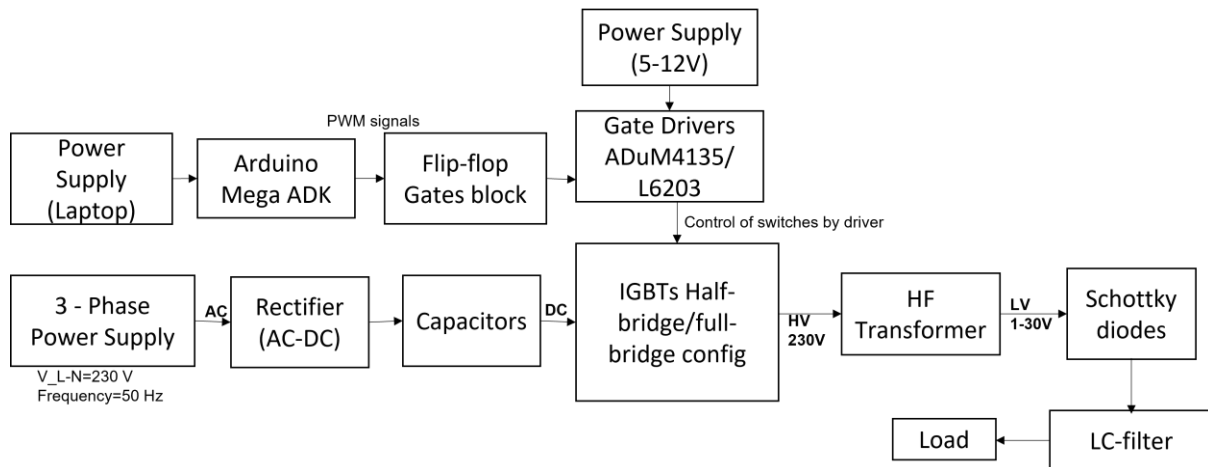
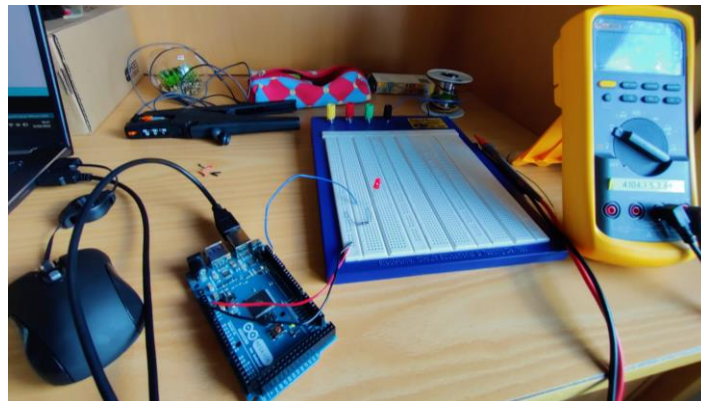Figure 4-3 Block diagram of the power supply system

Figure 4-4 LED brightness change with Arduino Mega ADK

4.2.1 Arduino Mega ADK

The Arduino Mega ADK with ATmega2560 is used to generate a PWM signal and the Arduino is powered by connecting to the laptop. Figure 4-5 shows the Arduino board with a power cable that can either be connected to the laptop USB port or the electric socket. It has 12 pins from 2 to 13 including supporting PWM waves. The PWM has a default frequency of $490\ Hz$ for all pins except for pins 13 and 4 which have a frequency of $980\ Hz$. The Arduino gives a square wave with $5\ V$ when it is High or $0\ V$ when it's low. Arduino IDE software is used to program and upload it to the Arduino board, where a program can be written to assign the pin number for PWM, change the frequency of PWM wave, change the duty cycle, etc. The Arduino IDE has a built-in function 'analogWrite()' which can be used to generate the PWM wave and the duty cycle of the wave can be changed using the same function. The value from $0 - 255$ can be given to the function where 0 represents the 0% duty cycle and 255 represents the 100% duty cycle. [32] [33]

The power supply circuit for MES requires higher frequencies of the PWM waves to switch the switches used in half-bridge/full-bridge converters, which can be programmed. In order to change the frequency on the pin value of the timer controlling the pin should be changed. There are five timers/registers on the board from timer 0 to timer 4, where timer 0 controls pin 13 and 4, timer 1 controls pin 12 and 11, timer 2 controls pin 10 and 9, timer 3 controls pin 5, 3, and 2, finally timer 4 controls pin 8, 7, and 6. The Arduino uses Prescaler, an eight-bit integer form 0-7 to generate the frequency for PWM. For all pins except 13 and 4, the maximum frequency is $31\ kHz$ with Prescaler 1 and the minimum frequency is less than $20\ Hz$ with Prescaler 6. In the case of timer 0 i.e., pin 13 and 4, the maximum frequency is $62\ kHz$ with Prescaler 1 and the lowest frequency is the same for all pins. The Prescaler 3 represents the default frequency value. For this case, the frequency of timer 1 has been changed to the Prescaler 1 i.e., $31\ kHz$ frequency. [34]
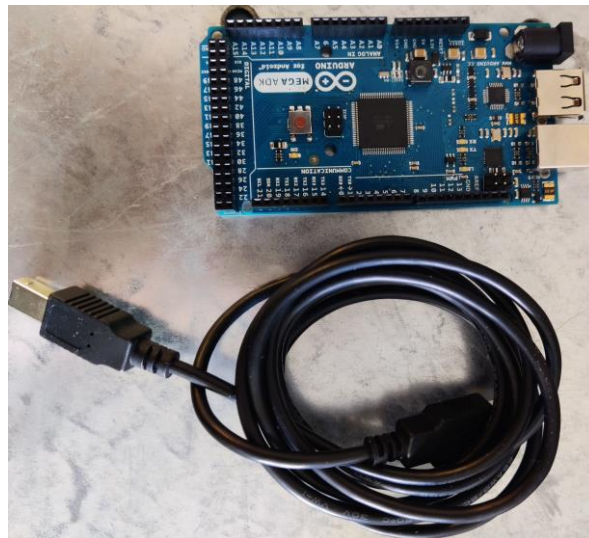

Figure 4-5 Arduino Mega ADK

4.2.2 Flip-flop Gates block

The AND gates and D flip-flop are required to control the switches in the power supply system. The working principle and utilization of the flip-flop and the gate are discussed in the subchapter 4.1.3. TC4013BP dual D-type flip flop is applied in the circuit which takes a supply voltage of $5\ V$ from pin 14 and the ground is pin 7. The outputs Q and Q! are taken from pin 1 and 2 respectively in the case. The clock signal is sent to pin 3, which is reversed PWM signal. TC4011BP quad 2 input NAND gates are used instead of AND gates to perform required operation. The power supply and the ground pin of the NAND gate are the same as the D flip-flop. All the NAND gates and the D flip-flop are powered by the Arduino. [35] [36]

Figure 4-6 shows the arrangement of the Arduino, D flip-flop, and NAND gates in the circuit which is powered by the Arduino supplying $5\ V$. Figure 4-7 shows the resulting signal from the flip-flop gate block with a duty cycle of 50%, where blue and yellow waveforms represent

the switching PWM signal with half switching frequency and half duty cycle. The switches take turns to be turned on every second time period when the PWM signal is high, which will be supplied to the switches.
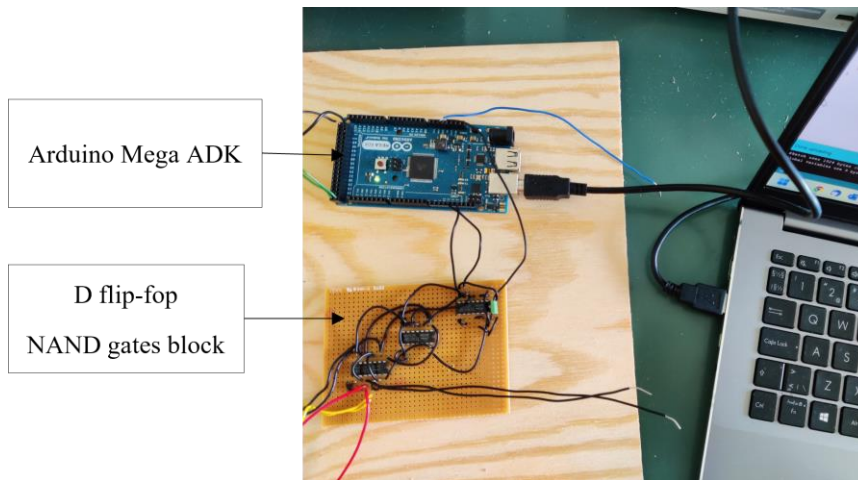
Figure 4-6 D flip-flop, NAND gate block
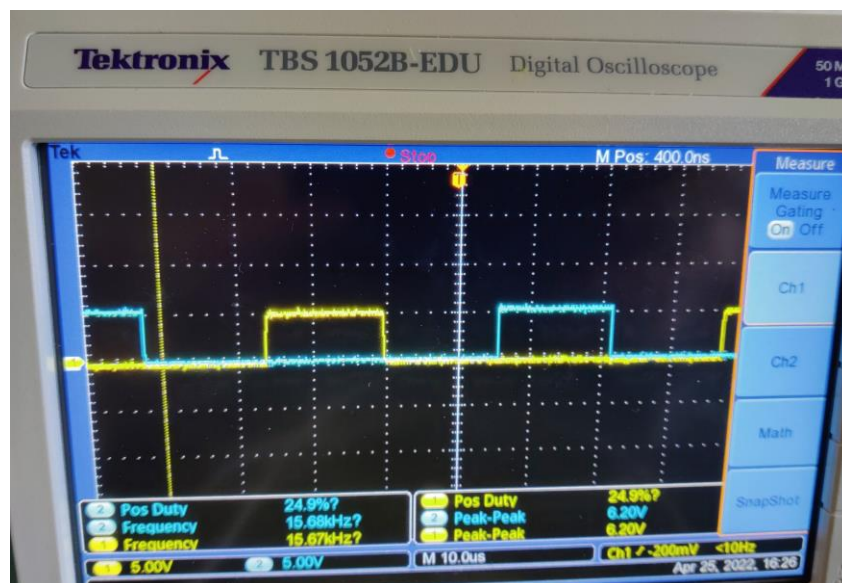
Figure 4-7 PWM signal generated to control switches

4.2.3 Gate Drivers

The gate driver sends switching signals to a gate of the transistors from the flip-flop gate block. In the beginning, the ADuM4135 single/dual-supply high voltage isolated gate driver was planned to use for all the switches, however, only one of the EVAL-ADuM4135 kits arrived during the circuit formulation so the L6203 DMOS full-bridge driver was used for driving other

switches. The L6203 driver does not have galvanic separation making it not preferable for the solution however it works fines for the testing purpose. On the other side, the ADuM4135 driver has analog devices chip-scale transformers to provide isolation and it also protects the IGBT from faults that may occur during operation [37]. Figure 4-8 shows the ADuM4135 driver kit and L6203 drivers.

The L6203 has the capacity to send gate signals to two switches from pins 1, 3, and 12 V power is supplied to pin 2 [38]. The ADuM4135 drives only one switch with isolated communication between the high and low voltage protecting the switch against high voltage. The logic side input is supplied from the Arduino and the high-side is supplied from the dc-power supply source to the respective pins as per the datasheet [37].
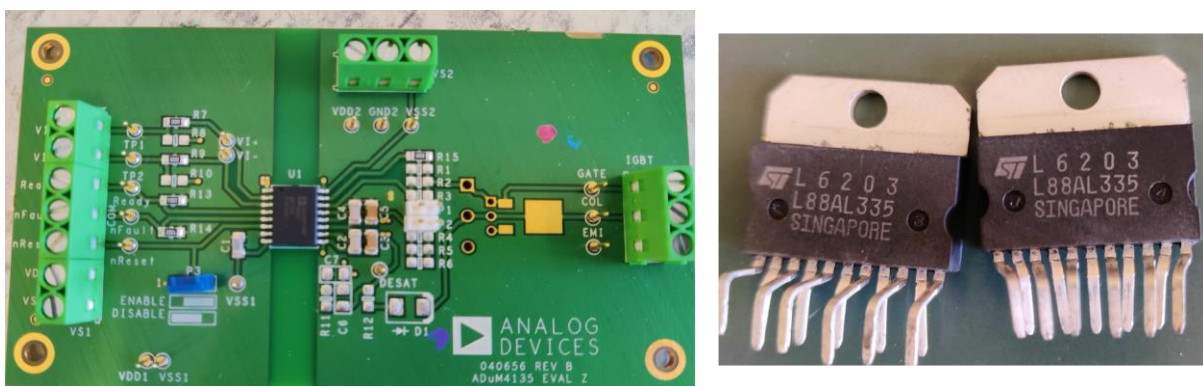

Figure 4-8 Gate drivers ADuM4135 and L6203

4.2.4 Rectifier

The three-phase rectifier MD75S16M4 applied to rectify given input voltage to dc voltage is displayed in figure 4-9. The working principle of the rectifier is described in the subchapter 3.1.1 and other details of the rectifier are given in the datasheet [39].

Figure 4-9 Three-phase rectifier MD75S16M4

4.2.5 Capacitors

Both low and high frequencies capacitor is applied in the power supply circuit as shown in figure 4-10. The capacitor bank with high-frequency capacitor C4AQ is used to reduce the input voltage ripple. As the switching frequency will be higher in the power supply model a polypropylene metalized film capacitor is used with $16\,\mu F$ capacitance, $\pm 10\%$ tolerance, $500\,V$ rated voltage, and a temperature range from $-55℃$ to $+105℃$ [40].
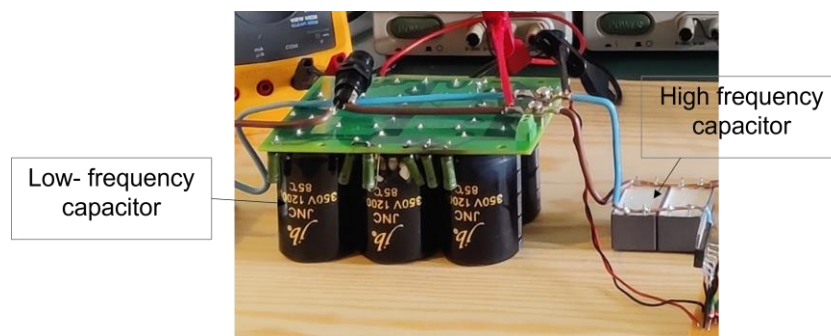
Figure 4-10 Low frequency and high-frequency capacitors

4.2.6 IGBTs

IGBTs are used for both half-bridge and full-bridge dc-dc converters as the voltage is higher on the input side of the system. The IGBT is more robust than MOSFET and it is suitable for switch-mode power supplies. To acquire an adequate safety margin $600\,V$, $125\,A$, $447\,W$ single switch mode IGBT is used, which can be operated at a higher switching frequency up to $150\,kHz$. Pins 1 and 4 represent emitter (E), 3 is a collector (C) and 2 is a gate (G) [41]. The warp 2 speed IGBT is displayed in figure 4-11.

Figure 4-11 IGBT (SOT-227)

4.2.7 Transformer Design

The transformer is designed according to the procedure described in the subchapter 3.1.7.2.

Step 1 Assemble design inputs

The input parameters required for the transformer design are in table 4-3. The transformer ratio is calculated from the known values of input voltage ($V_{d,max}$), output voltage (V_d) as follows:

$$transformer\ ratio\ (n) = \frac{V_{d,max}}{V_o,max} = \frac{400}{30} = 13.33$$

Hence the transformer ratio 16 is chosen instead of the nearest even number 14 so that there will be some margin space in case of a failure while designing the transformer.

Table 4-3: Parameters for the transformer design

Parameter	Value
Input Voltage (V_d)	360-400 V
Output Voltage (V_o)	20-30 V
Output Current (I_o)	100 A
Output Power (P_o)	2-3 kW
Switching Frequency (f)	31 kHz
Operating mode	Step-down
Duty cycle (D)	50%

Step 2 Choose core material, shape, and size

As the operating frequency is higher ferrite cores are selected and depending on the output power of the system and availability on the market during procuring period E65 type core is selected as in figure 4-12 [18]. During this step, a random size of the E65/32/27-3C94 core is selected and it will be updated after calculating the winding area required for the conductor. The core has an effective area A_c of $540\ mm^2$,saturation flux density B_{sat} of $0.32\ T$ and permeability µ of around 2300 [42].
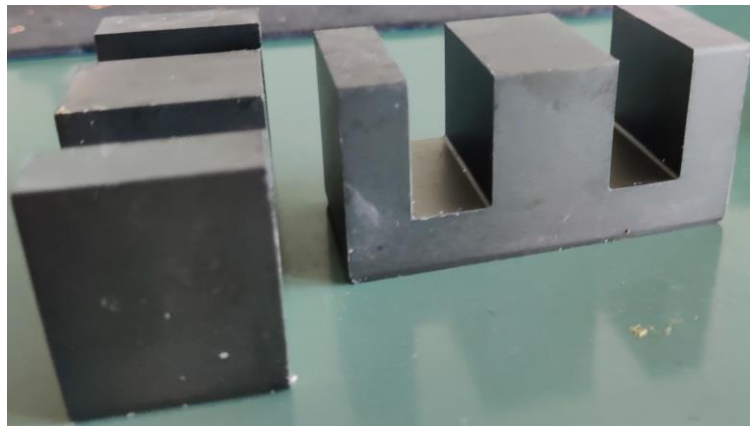

Figure 4-12 E65-type ferrite core

Step 3 Find the primary and secondary turns

The number of turns on the primary is calculated as per the equation (3.5) and the secondary turns are calculated according to the equation (3.6).

The number of turns on the primary side,

$$N_{pri} = \frac{400 * 0.5 * (\frac{1}{31 \times 10^3})}{540 \times 10^{-6} * 0.32} = 37.33 \approx 38$$

The number of turns on the secondary side,

$$N_{sec} = \frac{38}{16} = 2.375 \approx 3$$

On the primary side, the number of turns is adjusted to 48 to maintain the turn ratio of 16 with 3 turns on the secondary side.

Step 4 Choose wire

The most suitable wire for the winding is the Litz wire as the operating frequency of the transformer is high. The RMS currents on the primary and secondary side of the windings for full-bridge rectifier setup are calculated from equations (2.4) and (2.5).

On the primary side,

$$I_{1,RMS} = \frac{1}{16} * 100 * \sqrt{0.5} = 4.42 \approx 5\ A$$

Similarly, on the secondary side,

$$I_{2,RMS} = I_{3,RMS} = \frac{1}{2} * 100 * \sqrt{1.5} = 61.24\ A\ \approx 62\ A$$

The acquired Litz wire has 100 strands in one roll with a diameter $7mm$, a cross-sectional area $(A_{c,wire})$ 0.385 mm^2 and current density (J) is 3 A/mm^2 has been chosen for this design.

The number of strands in bundled wires required in the winding is calculated using the equations (3.7) and (3.9).

On the primary side,

$$X_{pri} = \frac{5}{3 * 0.385} = 4.32\ \approx 5\ strands$$

Similarly on the secondary side,

$$X_{sec} = \frac{62}{3 * 0.385} = 53.67 \approx 54 \; strands$$

Then, the new cross-sectional area of the wire on the primary and secondary sides is calculated as the equation (3.8) and (3.10).

On the primary side,

$$A_{c1,bundle} = 5 * 0.385 = 1.92 \; mm^2$$

On the secondary side,

$$A_{c1,bundle} = 54 * 0.385 = 20.79 \; mm^2$$

Step 5 Find the required winding window

The winding area on the primary and secondary sides of the transformer is calculated using the equations (3.11) and (3.12). The copper fill factor K_{cu} of 0.4 has been assumed to cater for both Litz wire and copper wire.

A winding area on the primary side,

$$A_{w,pri} = \frac{48 * 1.92}{0.4} = 230.4 \; mm^2$$

A winding area on the secondary side,

$$A_{w,sec} = \frac{3 * 20.79}{0.4} = 155.92 \; mm^2$$

Hence, the total winding area is calculated using equation (3.13),

$$A_w = 386.32 \; mm^2$$

Step 6 Calculate the winding window of the selected core

The winding area in the transformer is calculated as the dimensions provided in the datasheet [42].

Total winding area of the transformer,

$$= 2 * (22.20 * 12.1) = 537.24 \; mm^2$$

Step 7 Compare required and calculated winding window

The winding window of the core is more than 1.5 times greater than the required winding area, hence the core size is suitable for the transformer. Also, the core will not get saturated with the given voltage and current.

As per the availability of the core as well as coil former E 65/32/27 of N87 core, the material is used in the design of the transformer in this case. The core is ungapped and has an effective core area A_c of $535\ mm^2$ and saturation flux density B_{sat} of $0.32\ T$ [43]. This change in the core area does not have any significant effect on the calculation of the number of turns, hence using this core instead of 3C94 does not create issues. Figure 4-13 displays the coil former with the primary and secondary windings of the bundled Litz wires. As seen in the figure the bobbin has the capacity to hold two pairs of ferrite cores, thus reducing the number of turns is reduced to a $32:2$ ratio with the assumption that the core will not be saturated during operation. At first, a centrally tapped transformer with copper wire windings with 32 turns of 3 strands on the primary and 4 turns of 4 strands on the secondary side with a center tap is built to test the circuit and then a Litz wire transformer with calculated values is employed in the circuit while testing for high current. Figure 4-13 exhibits both centrally tapped transformers with copper wire and Litz wire assembled for the circuit testing.

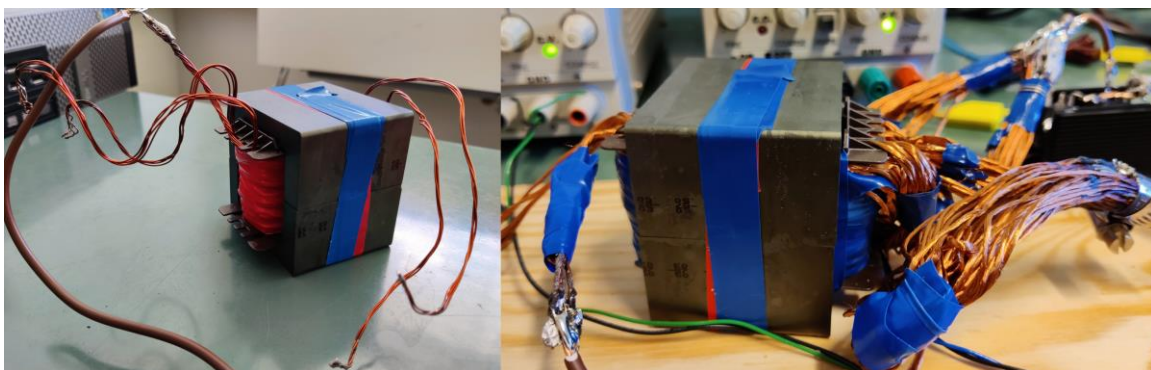Figure 4-13 Transformer windings with the Litz wire

Figure 4-14 Transformer with copper wire winding on left and Litz wire winding on right side

4.2.8 Schottky Diodes

Two Schottky diodes 200V 1120A T0257 are connected as a rectifier in the output of the secondary winding of the transformer. Figure 4-15 shows the diode where pin 1 represents the cathode and pin 2 is an anode. The diode has a maximum DC reverse voltage of $200V$, maximum average forward current of $120A$, and low leakage current and it is suitable for high switching frequency [44]. In the modeling of a power supply system with a half-bridge dc-dc converter, a fast recovery rectifier diode with reverse voltage 1 kV and forward current 30A is applied in the circuit [45]. A heat sink is also employed with two diodes to reduce the power loss in form of heat and prevents overheating by absorbing and dissipating heat generated by the diodes.

Figure 4-15 APT100S20BG high-voltage Schottky diode

4.2.9 LC Filters

An inductor and capacitor are connected to the output circuit as an LC filter to smoothen ripples of the rectified output voltage before passing to the load. For the inductor six winding of copper wire are wrapped around the bobbin and one pair of cores is used with a small air gap. The exact value is not calculated while building the model and tested with six winding inductor which worked fine so continued to use throughout the whole testing period. In the case of capacitors, two low-frequency and one high-frequency capacitor are used. Figure 4-16 displays the inductor and capacitor used in the power supply system. For the high current testing, the inductor is replaced by 5 turn winding of Litz wire.
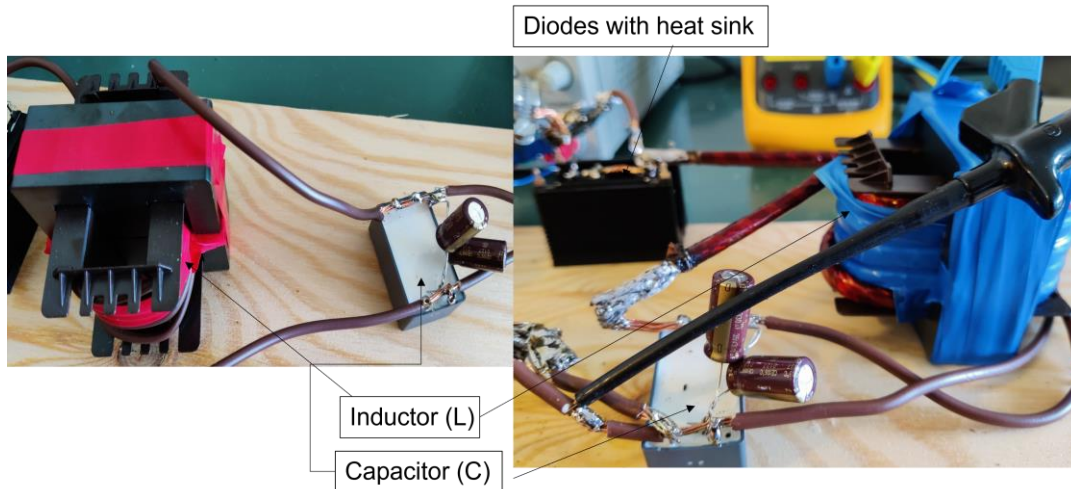
Figure 4-16: LC filter in the model

4.2.10 Load

A copper wire with resistance around $0.1 - 0.3 \, \Omega$ has been used during the testing of the circuit. According to the output voltage of $20 \, V$ and current of $100 \, A$, the resistance is $0.2 \, \Omega$. The length of the copper wire is calculated using equation (4.3) with the known diameter/radius of the wire. A roll of copper wire with resistance around $0.3 \, \Omega$ is used as a load for testing, which is kept in the bucket filled with water.

$$Resistance, R = \frac{\rho L}{A} \tag{4.3}$$

Where, ρ = resistivity of copper wire, $1.72 \times 10^{-8} \, \Omega m$

L = length of the wire

$A = \pi r^2$, cross-sectional area of the wire

Initially, the power supply system with a half-bridge dc-dc converter is built, tested, and then moved towards a full-bridge dc-dc converter system. At last, the power supply system is tested with a maximum single-phase input supply voltage of around $240 \, V$ to generate power of approximately $2000 \, W$ across a load of roughly $0.17 \, \Omega$.

5 Design Results and Discussion

The circuit is designed with components and specifications as explained in subchapter 4.2.

5.1 Power Supply System with Half-bridge DC-DC Converter

The power supply system with the half-bridge dc-dc converter is displayed in figure 5-1 which is tested with $30\ V$ input voltage supply and the transformer with copper wire. The turn ratio of the transformer is 6 and with the supply voltage of $30\ V$ and switching frequency of $31\ kHz$, the output voltage measured is around $1.8\ V$ at 50% duty cycle. As the input voltage is small, the rectified output voltage is also quite small, and it does not light up the bulb during this duty cycle. Figure 5-2 shows the waveform across one of the diode rectifiers. When the IGBT is on, the diode is conducting for half of the time period and when it is off the voltage across the diode decreases as the transformer core demagnetizes and reaches zero before conducting again.
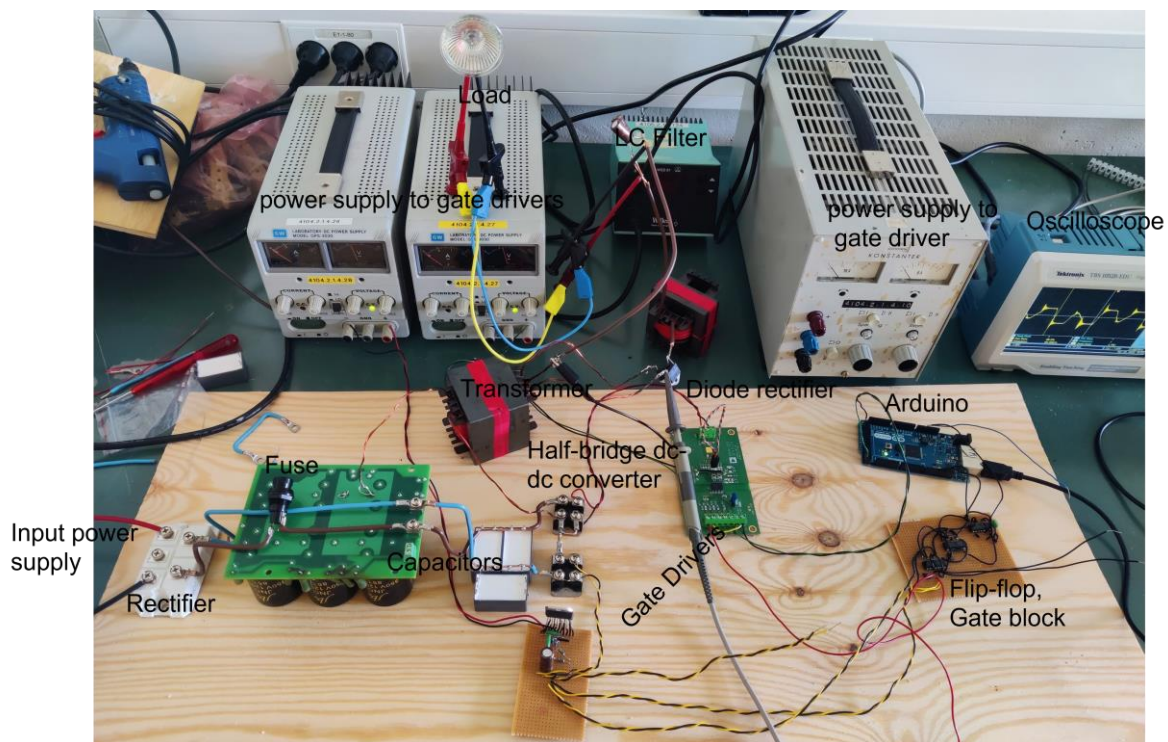

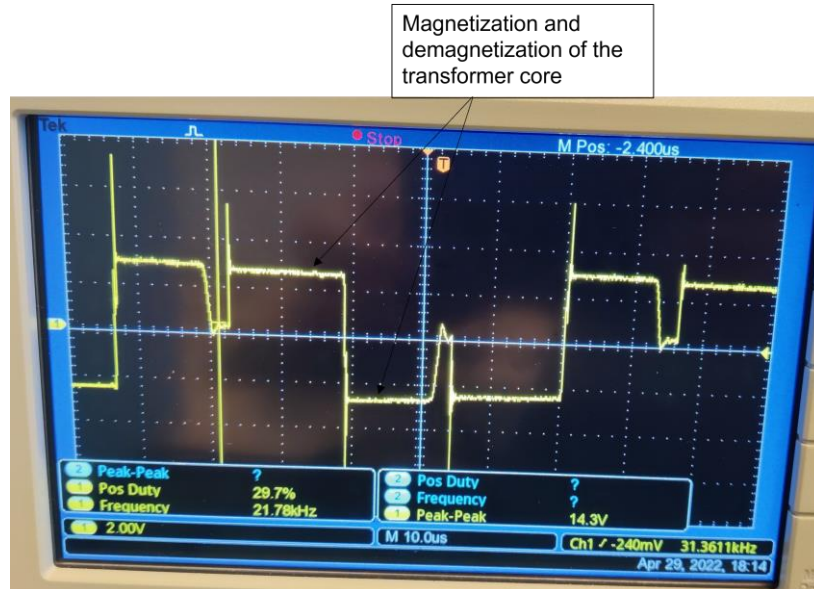Figure 5-1 Power supply system with half-bridge dc-dc converter

Figure 5-2 Output waveform across one diode rectifier

5.2 Power Supply System with Full-bridge DC-DC Converter

Initially, the full-bridge system is tested with a copper wire winding transformer having a turn ratio of 16 and powered by a single-phase variac which allowed voltage adjustment of the supply. For the load, a copper wire with resistance around 0.3 Ω is placed in the bucket filled with water and the switching frequency is 31 kHz. The power system model with a full-bridge dc-dc converter is displayed in figure 5-3.

The test started with an input voltage of 106.2 V with 25% duty cycle and a load of resistance of nearly 0.3 Ω. The expected output voltage is around 1.66 V, however, 1.3 V output voltage and 4.2 A current are measured across the load due to losses in the switches, transformer, and diodes. Figure 5-4 shows the waveforms observed on the primary and the secondary side of the transformer. The yellow waveform represents conduction on the primary side where on time is 25%, and the blue waveform shows the conduction on the secondary side with some noise during on time. The sharp shoot on the blue waveform illustrates noises during magnetization and demagnetization of the transformer core.

On the second test, the duty cycle is incremented to 50% with input voltage of 100.5 V. The output voltage across the load is measured to be 2.5 V. The transistors switch on and off at every half of the whole cycle. Figure 5-5 shows the signals across the transformer, where small oscillation on the primary side i.e., yellow waveform explains the magnetization of the core when the switches are on and then demagnetization when the switches turn off. At the same time, there are overshoots and undershoots on the secondary side i.e., the blue waveform of the transformer due to magnetic action. Afterward, the duty cycle is extended to 75% with an input voltage of 101.7 V and an expected output voltage of 4.8 V. The voltage and current across the

load are measured to be $3.9\,V$ and $12.6\,A$ due to losses on the secondary windings, rectifier diodes, and inductor. The waveform observed on both sides of the transformer is displayed in figure 5-6. Furthermore, an output voltage of $4.6\,V$ is observed with the duty cycle of 96% and input voltage $100\,V$. In this case, the signal on the primary side looks quite ideal and the magnetization action does not have a huge impact on the secondary side of the transformer as illustrated in figure 5-7.
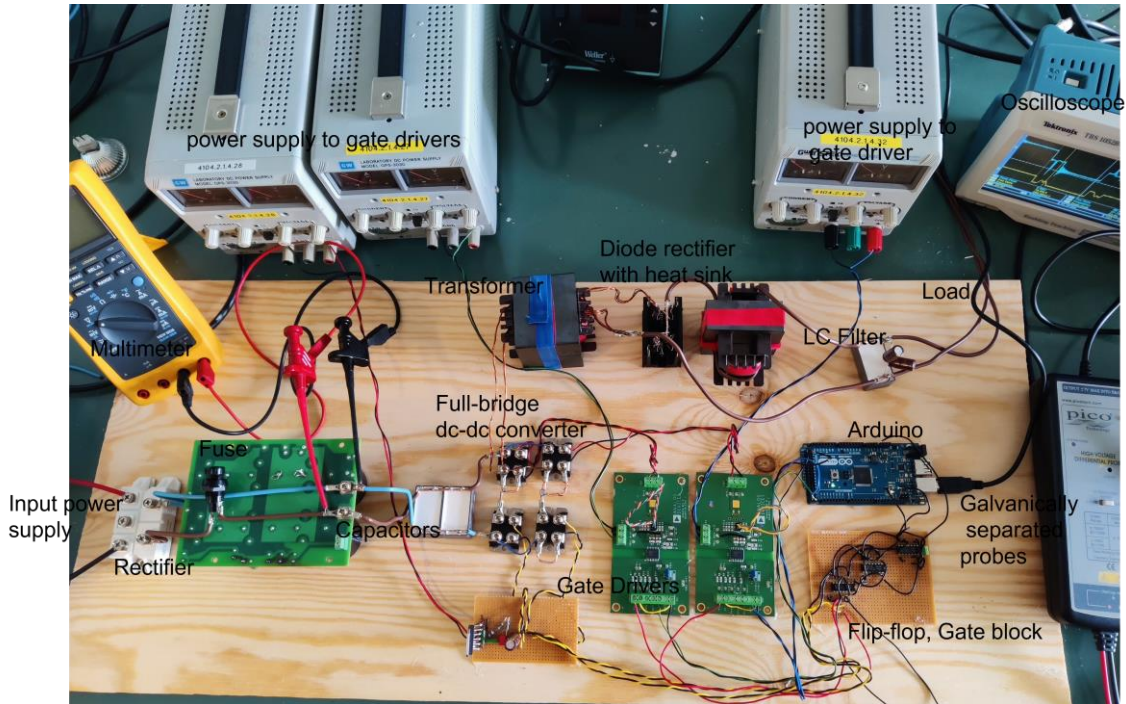

Figure 5-3 Power supply system with full-bridge dc-dc rectifier
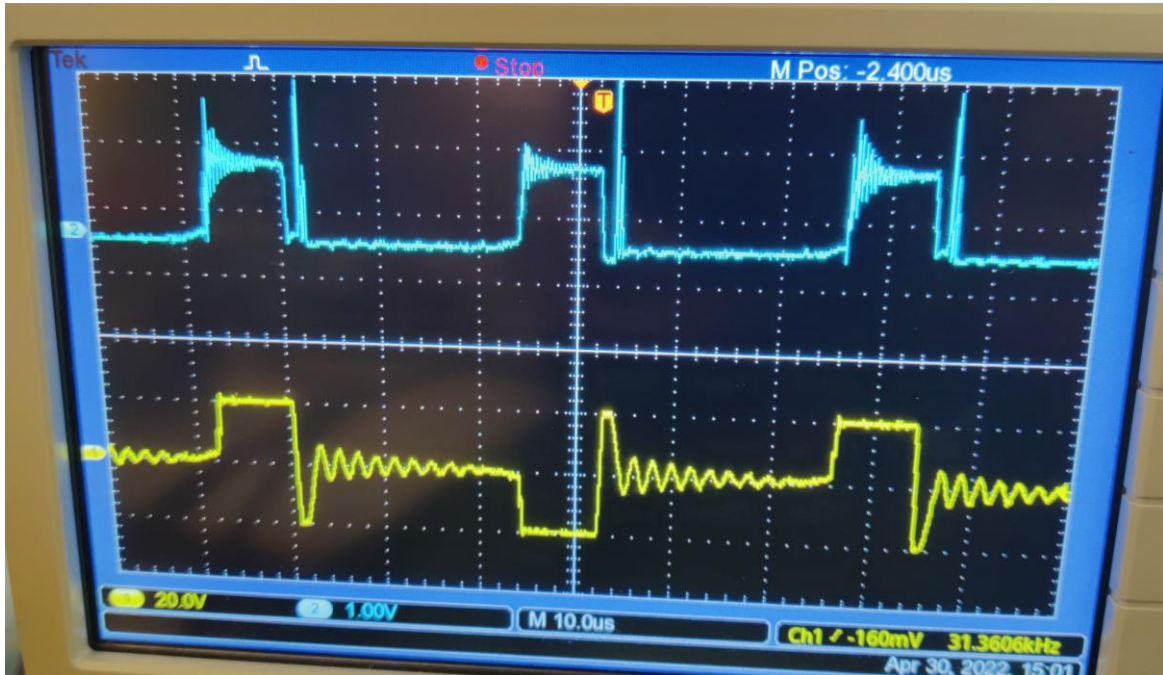
Figure 5-4 Waveforms on the primary (yellow) and the secondary side (blue) of the transformer with 25% duty cycle

Figure 5-5 Waveforms on the primary (yellow) and the secondary side (blue) of the transformer with 50% duty cycle

Figure 5-6 Waveforms on the primary (yellow) and the secondary side (blue) of the transformer with 75% duty cycle
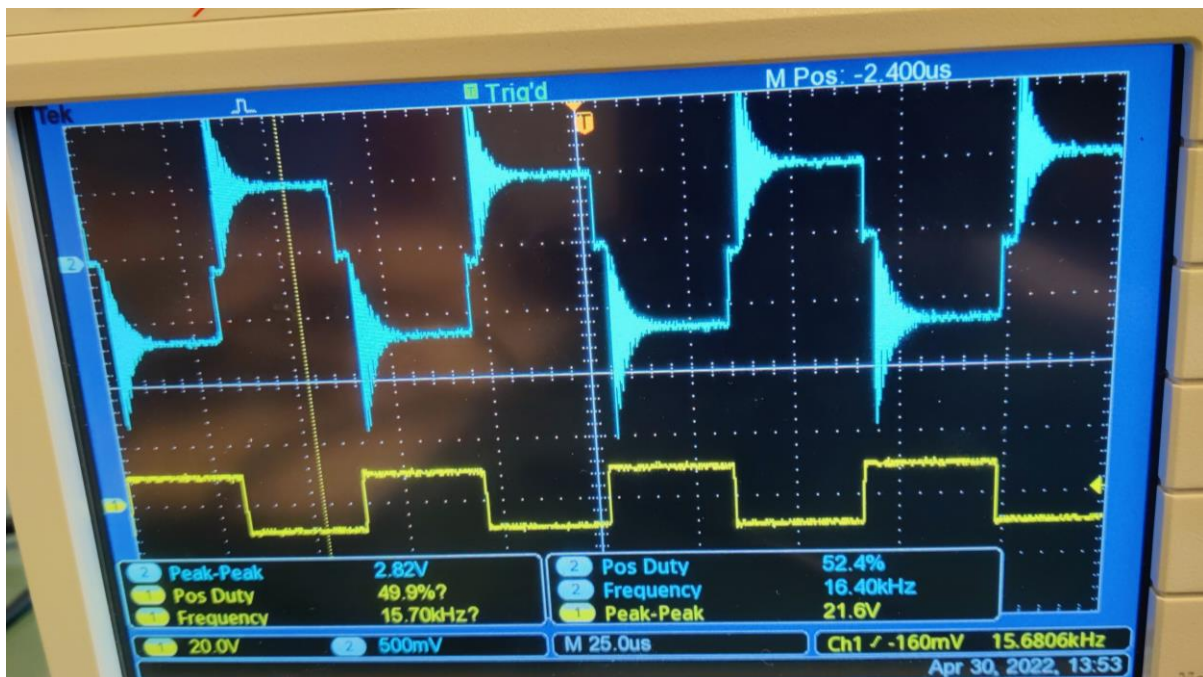

Figure 5-7 Waveforms on the primary (yellow) and the secondary side (blue) of the transformer with 96% duty cycle

After testing in the voltage around 100 V, the input level is increased, and the output measured across the load is in table 5-1. The power across the load rises with an ascent of input and duty cycle. The duty cycle is always maintained lower than 100%, creating a blanking time to avoid short-circuiting of the input. The wave on the primary side (yellow) almost looks like an ideal square wave and on the secondary side, (blue) oscillations happen when the IGBTs switch from off to on as shown in figure 5-8.

To check the saturation limit of the transformer core, the switching frequency is reduced to $490\ Hz$ and the duty cycle is amplified to 90%. The transformer saturates at $16V$ input voltage which concludes that the core saturation of the transformer occurs at approximately $1012V$ input voltage supply.

Table 5-1: Output of the system with different input and duty cycle

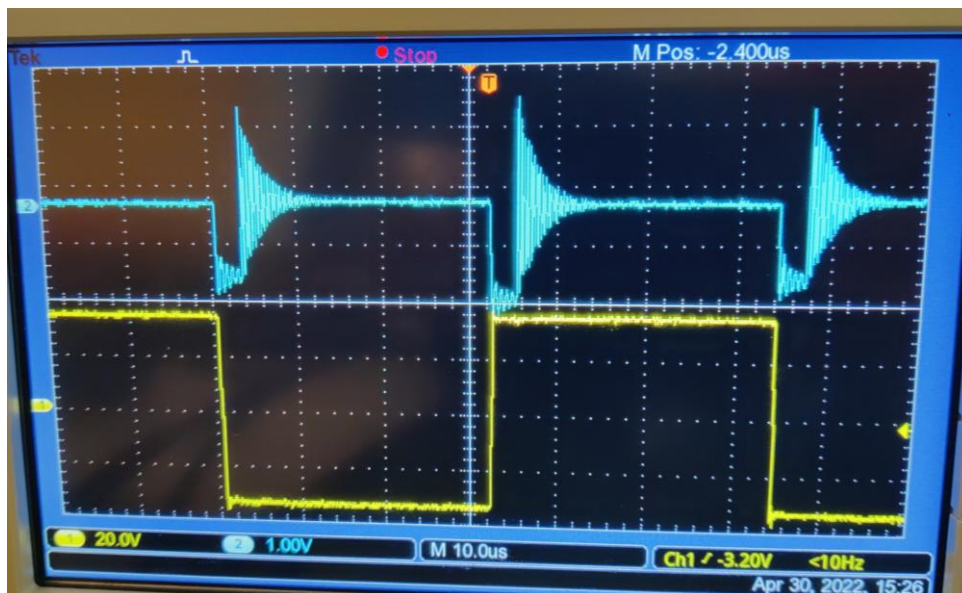| Measurement with a load of 0.3 Ω			
Duty cycle [%]	Input AC voltage [V]	Output DC voltage [V]	Output DC Current [A]
25	200.00	2.69	8.70
25	303.10	4.25	13.75
25	353.46	5.02	16.25
50	348.14	10.03	32.46
84	336.86	17.24	55.79

Figure 5-8 Waveforms on the primary (yellow) and the secondary side (blue) of the transformer with 84% duty cycle

Finally, testing on the circuit is conducted with the centrally tapped Litz wire winded transformer, the Litz wire winded inductor, and a load of resistance of 0.17Ω. The setup of the circuit is displayed in figure 5-9 and table 5-2 contains the output measured with different input and duty cycles. The output power escalates with the increase of the duty cycle and full power is attained at 100% duty cycle. At this level, the diode rectifier really gets heated up and transistors are also hot losing the power in the form of heat. The maximum single-phase input to the circuit is $250\ V$ and the current is $9\ A$ thus input power is around $2250\ W$ at the full duty cycle and the output power is nearly $1843\ W$. The efficiency of the model is almost 82%, whereas the same model shows an efficiency of 84% while simulating in the Simulink. It should be noted that the circuit is receiving supply from the single-phase and the use of the three-phase power supply will improve the output power of the circuit amplifying efficiency.
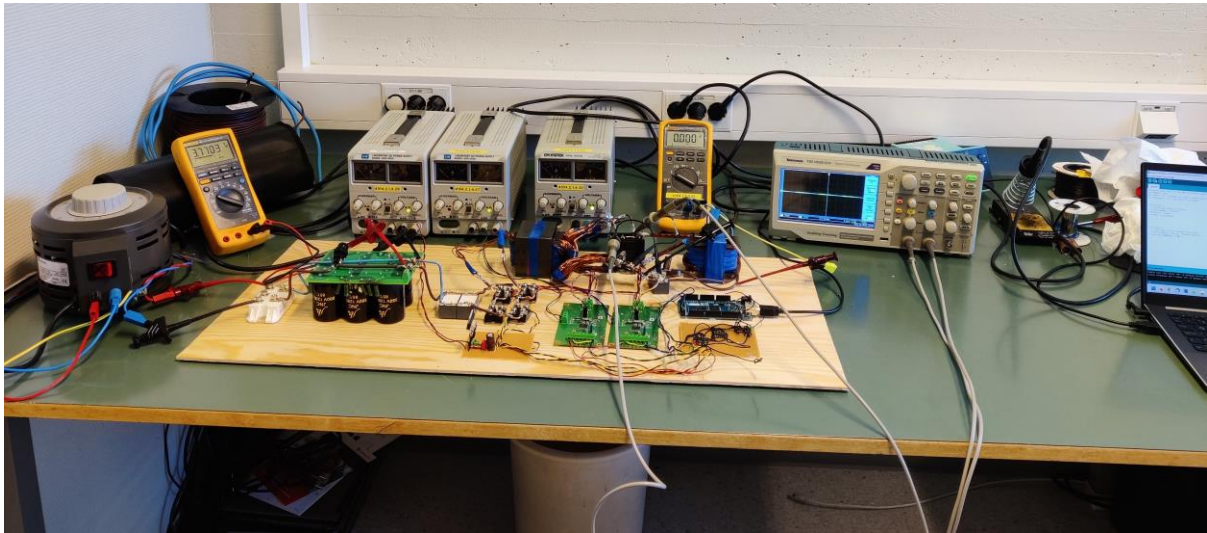

Figure 5-9 Power supply setup with the Litz wire winded transformer

Table 5-2: Measurements of output with high input supply

Measurement with a load of 0.17 Ω				
Duty cycle [%]	Single-phase Input DC voltage [V]	Output DC voltage [V]	Output DC Current [A]	Voltage Ratio [%]
10	356.0	1.9	11.2	0.53
20	352.2	3.8	22.4	1.08
30	349.6	5.8	34.1	1.66
40	346.0	7.5	44.1	2.17
50	341.8	9.6	56.5	2.81
60	339.0	10.9	64.1	3.22
70	334.0	12.6	74.1	3.77
80	330.1	14.8	87.1	4.48
90	325.2	16.4	96.5	5.04
100	322.2	17.7	104.1	5.49

Figure 5-10 illustrates the gradual expansion of the voltage across the load as the duty cycle increase with an interval of 10%. Simultaneously input dc voltage declines with a surge in the duty cycle as displayed in figure 5-11. The maximum input dc voltage is $356\,V$ at 10% duty cycle with the lowest output voltage close to $2\,V$, whereas the highest output voltage of roughly $18\,V$ is measured at duty cycle at about 100% and $322\,V$ input dc voltage. Figure 5-12 shows the plot of output to input dc voltage ratio against the duty cycle. Only 0.53% of input is transferred to the load when the duty cycle is minimum then the voltage ratio continuously grows with amplification of the duty cycle.
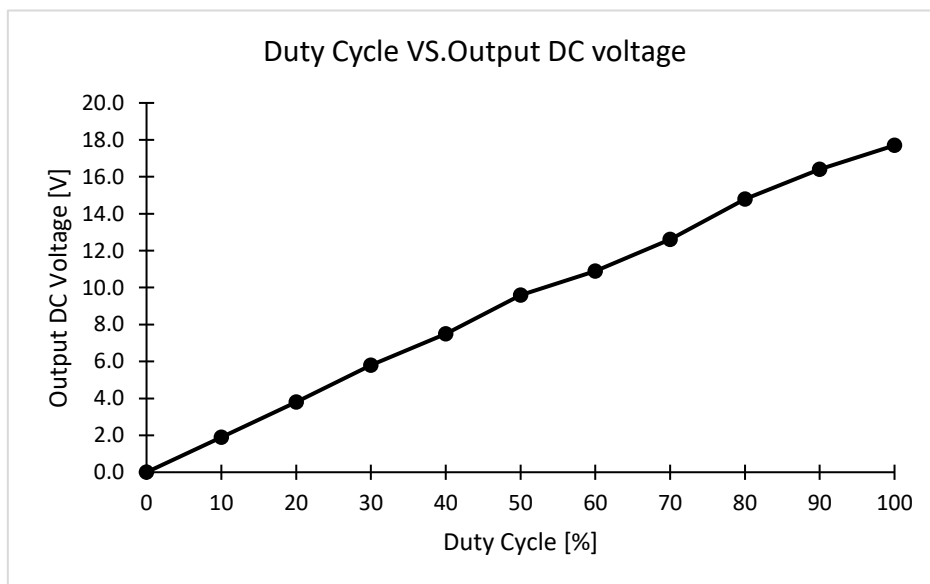

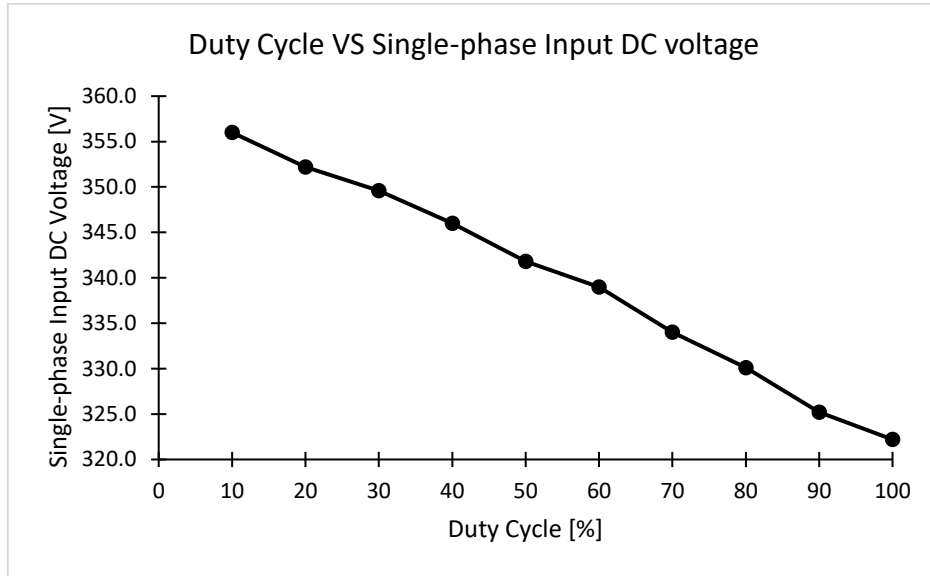Figure 5-10 Plot of duty cycle vs output voltage

Duty Cycle VS Single-phase Input DC voltage

Figure 5-11 Plot of duty cycle vs input dc voltage

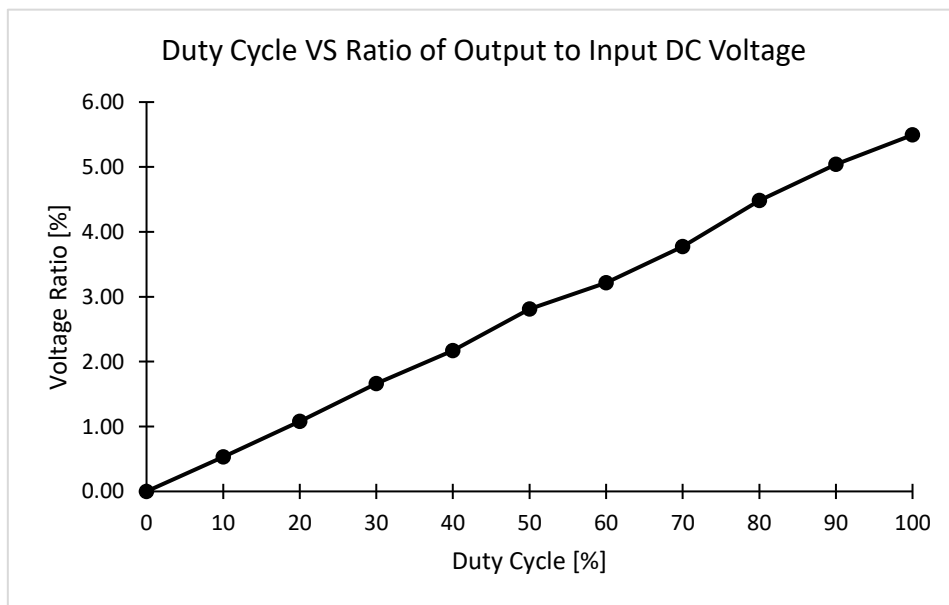## Duty Cycle VS Ratio of Output to Input DC Voltage

Figure 5-12 Plot of duty cycle vs voltage ratio

The power loss at the different components such as transistors, diode rectifiers, core, windings, inductor, capacitors, and connecting wires are not measured in this study, which accounts for not receiving expected voltage across the load and heating of transistors, diodes, and load. The loss on the circuit is approximately $407\,W$. Thermal images of the circuit are captured when the single-phase input supply is at the maximum level with the duty cycle at nearly 100%. The most heated part is the didoes on the output side, then the wire connected to the load as illustrated in figure 5-13. The Schottky diodes have a maximum forward voltage of $0.95\,V$ at

a forward current of around $100\ A$, therefore about $95\ W$ power is lost on the diodes in the form of heat as demonstrated by the thermal image. The rest of the power is lost on other components such as transistors, windings, inductors, capacitors, and cables connected to the load. The figure only displays temperature rise in the different equipment, yet the magnitude of loss is not determined.
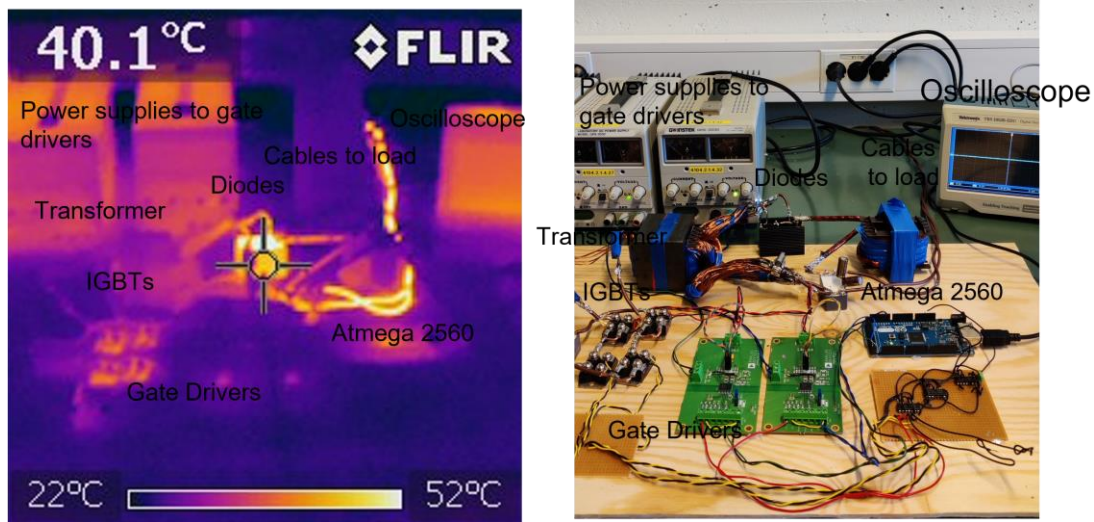

Figure 5-13 Thermal image of the power supply model

5.3 Evaluating the Scalability and Expansion for the full-scale Reactor Setup

For the scalability of the power supply system, the output voltage requirement will be assumed to be the same as for the lab-scale setup and the output current will increase depending upon the output power required for the full-scale setup.

As the scale of the setup increase, the power supply system should be able to supply higher current to the load which will lead to higher losses in the circuit. The power supply circuit is about 2% less efficient than the Simulink designed model, however, the efficiency may remain the same as the lab-scale model which is equivalent to 82% if it is increased linearly. Proper connecting wires, transformer winding, and a better cooling system for the circuit are required to minimize the losses. Also, the components including transistors, diodes, capacitors, inductors, transformers, connecting wires/cables, etc. should have the capacity to withstand high currents flowing across them.

6 Conclusion

MES uses electrodes and biofilm to produce methane or other valuable products from CO_2 and the process is electrically driven. As per the experiments conducted by the Department of Process, Energy, and Environmental Technology at USN, the biogas production system upgrades with the MES yield additional methane and reduced CO_2 than the normal system. This thesis work is concentrated on designing an optimal DC power supply system that can provide power to a lab-scale biochemical system setup.

Both the half-bridge and full-bridge dc-dc converter with electrical isolation is considered for the power supply model. The lab-scale MES setup requires a power of roughly $2 - 3\ kW$ with voltage of around $2 - 3\ V$, and current of nearly $1000\ A$, thus the full-bridge dc-dc converter is appropriate for the power supply system. Further, the model will be connected in a series configuration with 10 times higher voltage and 10 times lower current which will improve the efficiency and minimizes power loss in the circuit. The Arduino Mega ADK is implemented for generating PWM signals for switching. The IGBTs are employed for the dc-dc converter which is more robust and suitable for the model. The E-type centrally tapped transformer with ferrite core (N87) is formulated based on the known input and output parameters. The 3-phase rectifier bridge is used for rectification on the input side whereas the Schottky diodes are employed on the low voltage side along with the LC filter.

The power supply system with the full-bridge dc-dc converter is capable of supplying necessary power to the MES. The system operating at a switching frequency of $31\ kHz$ with maximum input from single-phase variac has an efficiency of 82% at full duty cycle whereas the full-bridge power supply system works with 84% efficiency on the Simulink. The efficiency of the circuit can be improved by supplying power from a three-phase power supply. The power losses in the circuit are not studied properly in this work, however, the thermal image of the system points out the majority of losses arise from the output side. As the Schottky diodes are losing energy, the application of MOSFETs/active rectifiers is recommended to lessen the losses across the rectifier. For the centrally tapped transformer, a double amount of winding is required on the low voltage side, therefore a larger core area compared to calculated values is suggested. Moreover, a proper cooling system is essential in the circuit.

6.1 Future work

The full-bridge dc-dc converter with electrical isolation has potential for implementation in the MES. However, the circuit can be upgraded to scale down power loss and enhance efficiency.

i.   Measurement of power loss in different components of the developed circuit and analysis of the components then replacement by better components.
ii.   Evaluation of the developed circuit with the correct value of inductance and capacitance for the LC filter and then with a three-phase ac power supply.

iii. Design of proper and compact circuit with cooling system for the components and proper connecting wires/cables suited for high current.

iv. Investigation of effects due to variations of output power in the electrosynthesis process of the MES.

v. Study of the efficiency of the MES with the implementation of a power supply system connected in a series configuration versus the use of only one power supply system capable of supplying desired power.

vi. Thorough research on the switch-mode power supply to the MES to expand the model for large-scale setup.

References

[1] 'Data & Statistics', *IEA*. https://www.iea.org/data-and-statistics/data-browser (accessed Feb. 24, 2022).

[2] K. Rabaey and R. A. Rozendal, 'Microbial electrosynthesis — revisiting the electrical route for microbial production', *Nat. Rev. Microbiol.*, vol. 8, no. 10, Art. no. 10, Oct. 2010, doi: 10.1038/nrmicro2422.

[3] S. Das, L. Diels, D. Pant, S. A. Patil, and M. M. Ghangrekar, 'Review—Microbial Electrosynthesis: A Way Towards The Production of Electro-Commodities Through Carbon Sequestration with Microbes as Biocatalysts', *J. Electrochem. Soc.*, vol. 167, no. 15, p. 155510, Jan. 2020, doi: 10.1149/1945-7111/abb836.

[4] B. E. Logan *et al.*, 'Microbial Electrolysis Cells for High Yield Hydrogen Gas Production from Organic Matter', *Environ. Sci. Technol.*, vol. 42, no. 23, pp. 8630–8640, Dec. 2008, doi: 10.1021/es801553z.

[5] C. A. Hernandez and J. F. Osma, 'Microbial Electrochemical Systems: Deriving Future Trends From Historical Perspectives and Characterization Strategies', *Front. Environ. Sci.*, vol. 8, 2020, Accessed: Feb. 24, 2022. [Online]. Available: https://www.frontiersin.org/article/10.3389/fenvs.2020.00044

[6] V. Sundling, 'Design of a Low-Voltage High-Power DC Power Supply for Microbial Electrochemical Synthesis', *63*, 2020, Accessed: Mar. 22, 2022. [Online]. Available: https://openarchive.usn.no/usn-xmlui/handle/11250/2688588

[7] 'Voltage Fed Full Bridge DC-DC and DC-AC Converter for High-Frequency Inverter Using C2000'. Accessed: Mar. 22, 2022. [Online]. Available: https://www.ti.com/lit/an/sprabw0d/sprabw0d.pdf?ts=1647942648506&ref_url=https%253A%252F%252Fwww.google.com%252F

[8] 'Linear vs Switching Power Supplies', *Advanced Conversion Technology*. https://www.actpower.com/educational/linear-vs-switching-power-supplies/ (accessed Feb. 24, 2022).

[9] N. Mohan, *Power electronics: converters, applications, and design*, 3rd ed. Hoboken, N.J: Wiley, 2003.

[10] 'Power Supply Technology - Half-Bridge DC/DC Converters| Mouser Electronics'. https://no.mouser.com/applications/power-supply-topology-half/ (accessed Mar. 10, 2022).

[11] 'Bridge Converter', *Sunpower UK*. https://www.sunpower-uk.com/glossary/what-is-a-bridge-converter/ (accessed Mar. 10, 2022).

[12]   M. H. I. Saif, 'Pilot Design of a Bioelectrochemical MES Wastewater Reactor', *67*, 2020, Accessed: Mar. 14, 2022. [Online]. Available: https://openarchive.usn.no/usn-xmlui/handle/11250/2688918

[13]   'rectifier | Types, Definition, & Facts | Britannica'. https://www.britannica.com/technology/rectifier (accessed Apr. 04, 2022).

[14]   'MOSFET and Metal Oxide Semiconductor Tutorial', *Basic Electronics Tutorials*, Sep. 03, 2013. https://www.electronics-tutorials.ws/transistor/tran_6.html (accessed Mar. 29, 2022).

[15]   'Insulated Gate Bipolar Transistor or IGBT Transistor', *Basic Electronics Tutorials*, Aug. 26, 2013. https://www.electronics-tutorials.ws/power/insulated-gate-bipolar-transistor.html (accessed Apr. 01, 2022).

[16]   'Arduino - Products'. https://www.arduino.cc/en/Main/Products (accessed Apr. 04, 2022).

[17]   'Arduino Mega ADK Rev3 | Arduino Documentation'. https://docs.arduino.cc/retired/boards/arduino-mega-adk-rev3 (accessed Apr. 04, 2022).

[18]   B. Madhaiyan, '12 Steps for Designing SMPS Transformers', *The Talema Group*, Sep. 26, 2018. https://talema.com/smps-transformer-design/ (accessed Apr. 05, 2022).

[19]   'Litz Wire: An Ideal Solution for High-Frequency Applications', *Agile Magnetics, Inc.*, Aug. 03, 2017. https://www.agilemagco.com/blog/5-benefits-of-using-litz-wire/ (accessed Apr. 06, 2022).

[20]   B. Madhaiyan, '12 Steps for Designing SMPS Transformers', *The Talema Group*, Sep. 26, 2018. https://talema.com/smps-transformer-design/ (accessed Apr. 06, 2022).

[21]   C. Andersson, 'Design of a 2.5kW DC/DC fullbridge converter', 2011, Accessed: Apr. 06, 2022. [Online]. Available: https://odr.chalmers.se/handle/20.500.12380/173958

[22]   'LC Filter for Power Supply Design Tips'. https://resources.pcb.cadence.com/blog/lc-filter-for-power-supply-design-tips (accessed Apr. 12, 2022).

[23]   'Transformer Losses | The Electricity Forum'. https://www.electricityforum.com/iep/electrical-transformers/transformer-losses (accessed Apr. 18, 2022).

[24]   'What is Matlab'. https://cimss.ssec.wisc.edu/wxwise/class/aos340/spr00/whatismatlab.htm (accessed Apr. 18, 2022).

[25]   'Simscape Electrical Block Libraries - MATLAB & Simulink - MathWorks Nordic'. https://se.mathworks.com/help/physmod/sps/ug/simscape-electrical-block-libraries.html (accessed Apr. 18, 2022).

References

[26] 'Simscape Documentation - MathWorks Nordic'. https://se.mathworks.com/help/physmod/simscape/index.html (accessed Apr. 18, 2022).

[27] 'Environment block for Simscape Electrical Specialized Power Systems models - Simulink - MathWorks Nordic'. https://se.mathworks.com/help/physmod/sps/powersys/ref/powergui.html (accessed Apr. 20, 2022).

[28] 'Implement diode model - Simulink - MathWorks Nordic'. https://se.mathworks.com/help/physmod/sps/powersys/ref/diode.html?s_tid=srchtitle (accessed Apr. 20, 2022).

[29] 'Implement MOSFET model - Simulink - MathWorks Nordic'. https://se.mathworks.com/help/physmod/sps/powersys/ref/mosfet.html?s_tid=srchtitle (accessed Apr. 20, 2022).

[30] 'Implement insulated gate bipolar transistor (IGBT) - Simulink - MathWorks Nordic'. https://se.mathworks.com/help/physmod/sps/powersys/ref/igbt.html (accessed Apr. 28, 2022).

[31] 'Implement two- or three-winding linear transformer - Simulink - MathWorks Nordic'. https://se.mathworks.com/help/physmod/sps/powersys/ref/lineartransformer.html?s_tid=s r (accessed Apr. 20, 2022).

[32] 'ArduinoMega2560Datasheet.pdf'. Accessed: Apr. 29, 2022. [Online]. Available: https://www.robotshop.com/media/files/PDF/ArduinoMega2560Datasheet.pdf

[33] 'Arduino PWM Tutorial', *Arduino Project Hub*. https://create.arduino.cc/projecthub/muhammad-aqib/arduino-pwm-tutorial-ae9d71 (accessed Apr. 29, 2022).

[34] 'mega 2560 PWM frequency - Using Arduino / Project Guidance', *Arduino Forum*, Sep. 14, 2011. https://forum.arduino.cc/t/mega-2560-pwm-frequency/71434/2 (accessed Apr. 29, 2022).

[35] 'TC4013BP_datasheet_en_20140301-963976.pdf'. Accessed: Apr. 29, 2022. [Online]. Available: https://no.mouser.com/datasheet/2/408/TC4013BP_datasheet_en_20140301-963976.pdf

[36] 'TC4011BP_datasheet'. Accessed: Apr. 29, 2022. [Online]. Available: https://docs.rs-online.com/97ff/0900766b8082ef4a.pdf

[37] 'ADuM4135.pdf'. Accessed: May 01, 2022. [Online]. Available: https://www.analog.com/media/en/technical-documentation/data-sheets/ADuM4135.pdf

[38] 'L6203 STMicroelectronics | Mouser', *Mouser Electronics*. https://no.mouser.com/ProductDetail/511-L6203 (accessed May 11, 2022).

[39]   'mccc_s_a0005071000_1-2274676.pdf'. Accessed: May 01, 2022. [Online]. Available:
https://no.mouser.com/datasheet/2/258/mccc_s_a0005071000_1-2274676.pdf

[40]   'C4AQLLW5160A33K.pdf'. Accessed: May 01, 2022. [Online]. Available:
https://connect.kemet.com:7667/gateway/IntelliData-
ComponentDocumentation/1.0/download/datasheet/C4AQLLW5160A33K

[41]   'VS-GB100DA60UP.pdf'. Accessed: May 01, 2022. [Online]. Available:
https://media.digikey.com/pdf/Data%20Sheets/Vishay%20Semiconductors/VS-
GB100DA60UP.pdf

[42]   'E65_32_27.pdf'. Accessed: May 01, 2022. [Online]. Available:
https://www.ferroxcube.com/upload/media/product/file/Pr_ds/E65_32_27.pdf

[43]   'Ferrites and accessories - E 653227 - Core and a.pdf'. Accessed: May 01, 2022.
[Online]. Available: https://www.farnell.com/datasheets/3158414.pdf

[44]   'APT100S20B Datasheet by Microchip Technology | Digi-Key Electronics'.
https://www.digikey.no/en/htmldatasheets/production/84049/0/0/1/apt100s20b.html?site=
US&lang=en&cur=USD (accessed May 11, 2022).

[45]   'BYT30PI-1000   STMicroelectronics | Mouser',   *Mouser   Electronics*.
https://no.mouser.com/ProductDetail/N-A (accessed May 11, 2022).

Appendices

Appendix A: Signed problem description for this master's Thesis

USN University of
South-Eastern Norway

Faculty of Technology, Natural Sciences and Maritime Sciences, Campus Porsgrunn

FMH606 Master's Thesis

Title: Design and Control of a DC Power Supply for Microbial Electrochemical Synthesis (MES)

USN supervisor: Kjetil Svendsen

External partner: - Environmental Biotechnology Research Group, USN-PEM

Task background:
Microbial electrochemical synthesis (MES) is a novel technology combining electrical, environmental, and chemical engineering disciplines. MES is a power to gas technology that seeks to convert carbon dioxide (CO_2) into organics that can be used as fuels or building blocks for new products to replace the use of fossil oil and gas. We have demonstrated such experimentally by biogas upgrading where biogas CO_2 is reduced to methane (CH_4), to increase the methane content in biogas produced by treatment plants. It uses electricity as an energy source and microorganisms as the catalyst for the chemical reduction reaction (CO_2 to CH_4) at the cathode in a methane-producing microbial electrolysis cell (MEC). This (thesis) task focuses on electricity/power supply to such a MEC with multiple electrodes installed in a single reactor compartment. USN has bioelectrochemistry as a research focus. USN has published research work and has laboratory facilities that will be the baseline for this project.

Task description:
Establish the framework and main parameters for power supply to a MES connected to an existing laboratory scale Anaerobic Digestion (AD) reactor.

As part of the thesis a low-voltage high-power DC power supply shall be designed:
- Literature research into half bridge and full bridge DC converters, transformers, and active rectifiers.
- Design of the half bridge DC-DC converter with electrical isolation power supply that can be used for a small-scale laboratory setup (size to be determined in cooperation with students and staff working on other design aspects).
- Modelling and simulation of the power supply with a simulation software.
- Control and optimization of the power supply output by reducing losses in the system.
- Build the power supply system operatable at low voltage and perform relevant tests with reactor if enough time is available.
- Evaluating the scalability and expansion of the found solution for the full-scale reactor setup.

Student category: EPE

Practical arrangements: -

Supervision:

ISN University of
South-Eastern Norway

Faculty of Technology, Natural Sciences and Maritime Sciences, Campus Porsgrunn

As a general rule, the student is entitled to 15-20 hours of supervision. This includes necessary time for the supervisor to prepare for supervision meetings (reading material to be discussed, etc).

Signatures:

Supervisor (date and signature):

1/2 22 *Kjchllegh*

Student (write clearly in all capitalized letters):

ELISHA THAPA , 01 Feb, 2022

Student (date and signature):

1-02-22

Appendix B: Duty cycle of PWM changing code of the Arduino

```
//Chaning duty cycle of the PWM via Arduino Mega ADK

int PWMPin = 12;

int erase = 7;  //binary 111 used to erase first 3 bits CS02,CS01,CS00

int prescale = 1; // for timer 2 i.e 31kHz



void setup() {

  // Declaring ledPin as output

  pinMode(PWMPin, OUTPUT);

  TCCR1B &= ~erase;

  TCCR1B |= prescale;



}



void loop() {

  //Duty cycle can be changed from 0-255,

  //0%=0, 10%=26, 20%=51, 30%=77, 40%=102, 50%=128, 60%=153, 70%=179, 80%=204,
90%=230, 100%=250

  analogWrite(PWMPin, 204);

}
```

Appendix C: Electric components and their arrangements

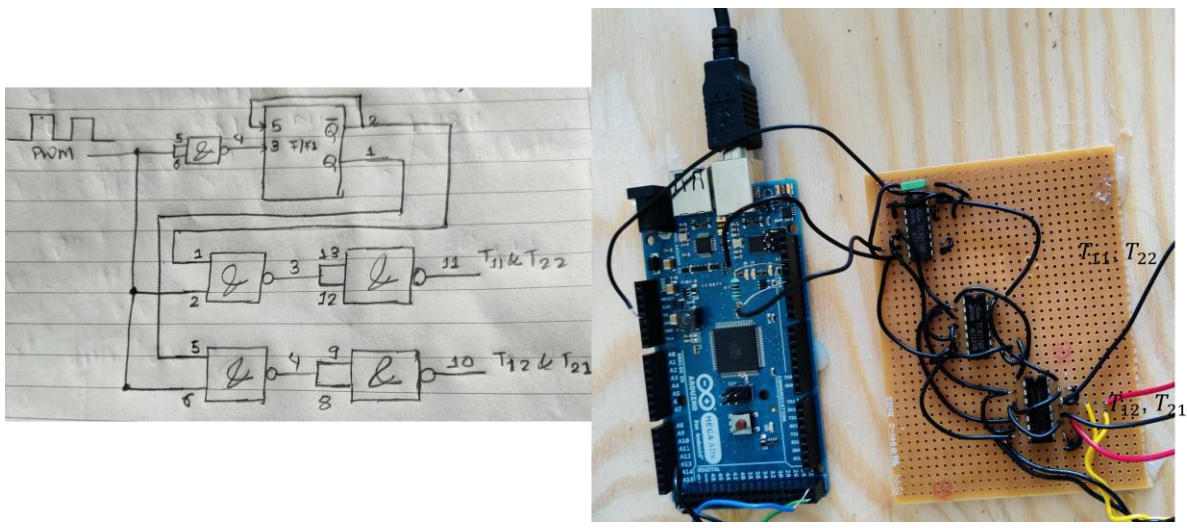1. Some of the components of the power supply model
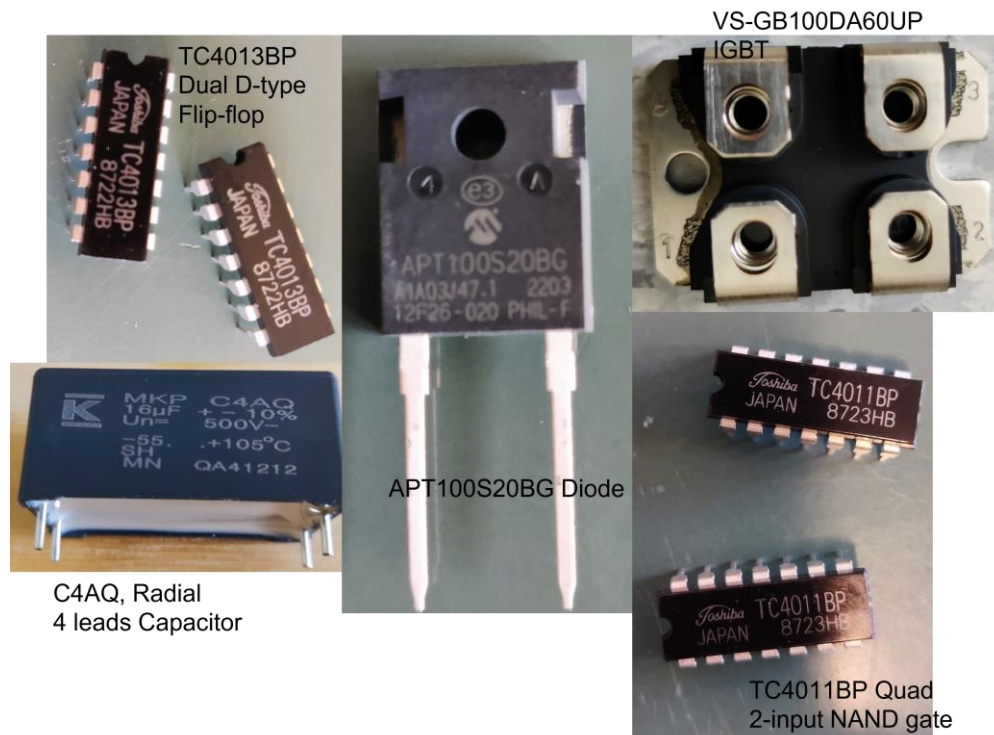
2. Arrangement of the Arduino, flip-flop, and gate block and measurement of PWM waves generated.
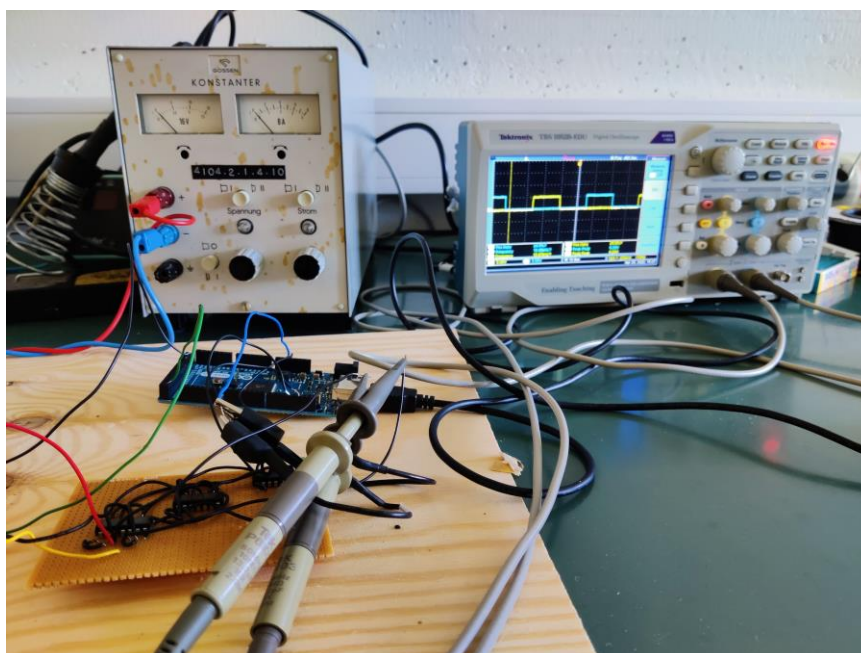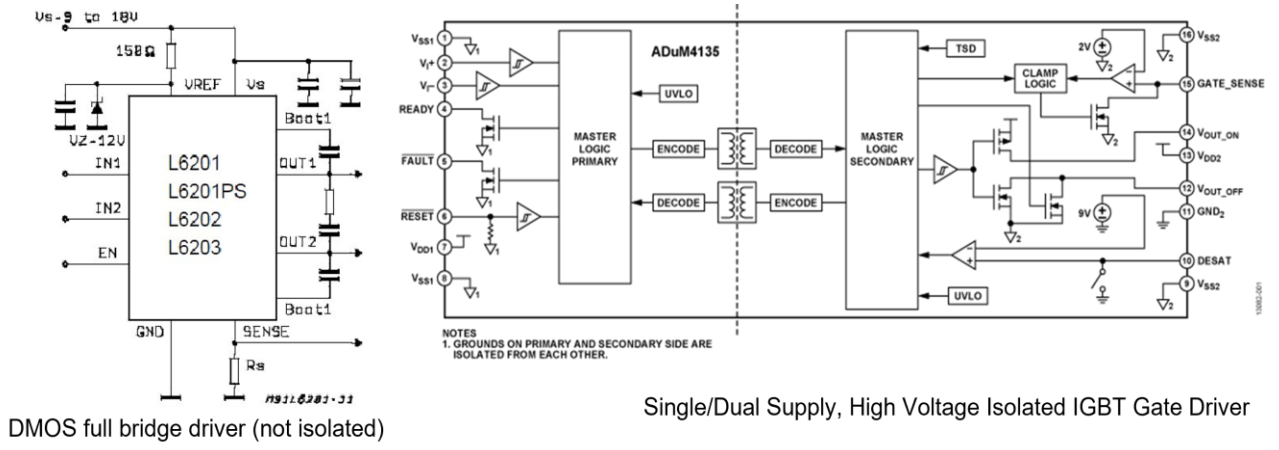
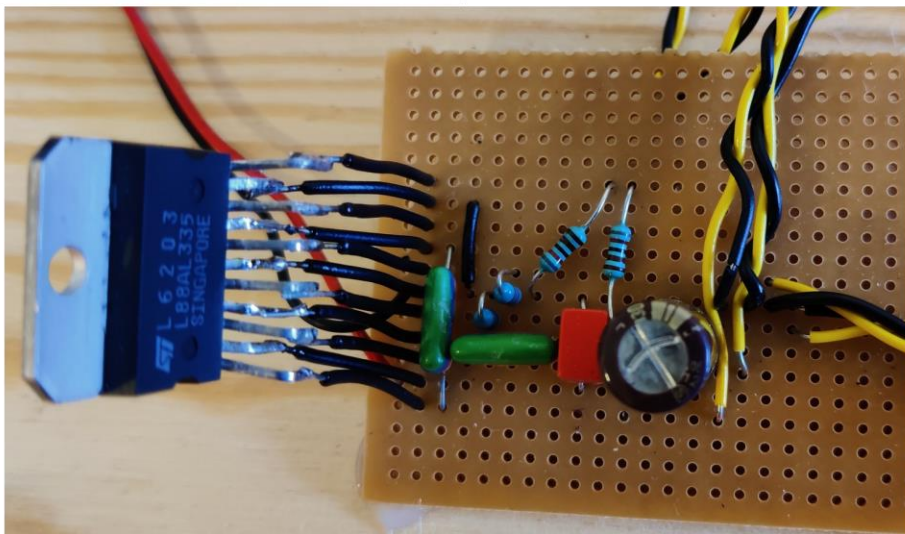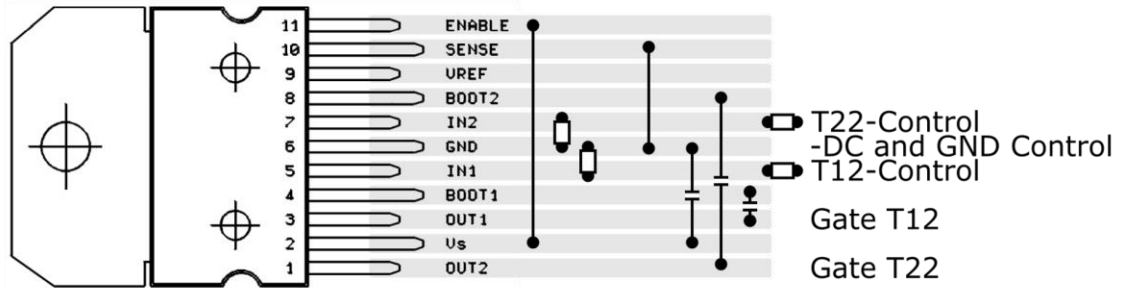3. Functional diagram of D flip-flop and NAND gates as per datasheet. [35] [36]

CD4013B CMOS Dual D-Type Flip-flop

CD4011B CMOS NAND Gate
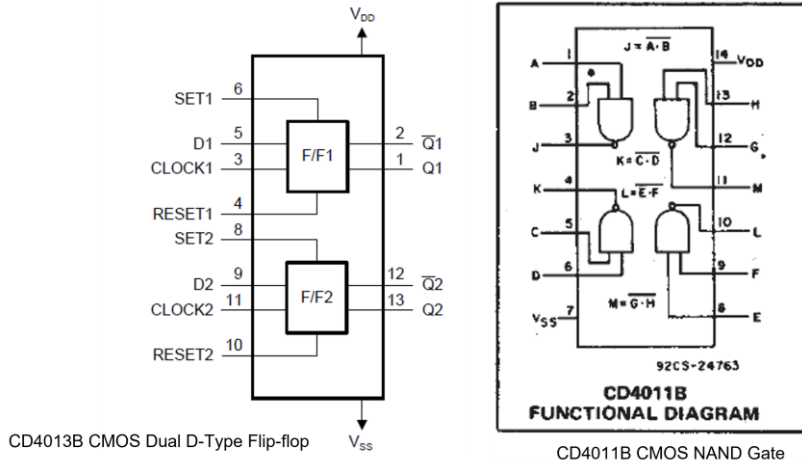
4. Arrangement of Flip-flop NAND gate block in the circuit.

5. Functional Diagram of gate drivers as per data sheet. [38] [37]

DMOS full bridge driver (not isolated)

Single/Dual Supply, High Voltage Isolated IGBT Gate Driver

6. Arrangement of the L6203 driver board for the power supply system

7. Arrangement of the power supply model with the half-bridge dc-dc rectifier
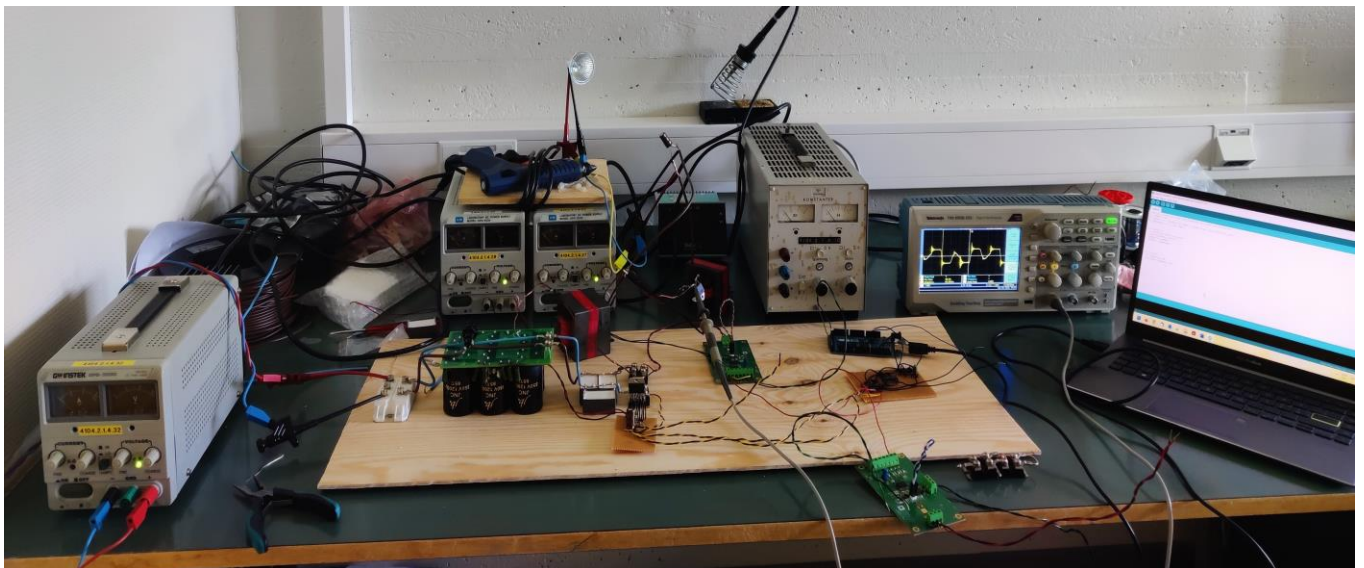
8. Arrangement of the power supply model with the full-bridge dc-dc rectifier